

# Altermagnetism and Superconductivity: A Short Historical Review

Zhao Liu,<sup>1,\*</sup> Hui Hu,<sup>1</sup> and Xia-Ji Liu<sup>1</sup>

<sup>1</sup>Centre for Quantum Technology Theory, Swinburne University of Technology, Melbourne 3122, Australia

(Dated: October 13, 2025)

This article explores the deep interconnections among three seemingly unrelated concepts in condensed matter physics: electronic liquid crystal phases, multipole expansions, and altermagnetism. At the heart of these phenomena lies a shared foundation: spin-momentum locking in the non-relativistic regime. Originally proposed in the context of electronic liquid crystal phases, spin-momentum locking was later elegantly incorporated into the formalism of multipole expansions. This framework can be further extended across multiple atomic sites, making it particularly effective for describing altermagnets, which feature localized magnetic moments distributed over at least two sublattices. In the second part of the article, we examine superconducting phenomena that stem from this shared mechanism, focusing on superconductivity in systems with spin-momentum locked Fermi surfaces. We highlight a rich variety of unconventional superconducting states, including finite-momentum pairing,  $d$ -wave and spin-triplet superconductivity, and topological Bogoliubov Fermi surfaces, among others. Additional related topics are addressed in the concluding section. Overall, this work offers both an accessible introduction to the newly identified magnetic order known as altermagnetism and a conceptual guide for researchers aiming to harness the ensuing unconventional superconductivity in the development of future quantum technologies.

Keywords: altermagnetism; multipole expansions; electronic liquid crystal phases; superconductivity

## I. INTRODUCTION

In recent years, there has been a growing surge of interest in a newly discovered magnetic order known as altermagnetism (AM)<sup>1–5</sup>. Although several excellent reviews have explored this rapidly evolving topic<sup>6–11</sup>, less attention has been given to the historical development of the underlying ideas, methodologies, and conceptual shifts that have defined the field. In this paper, we aim to shed light on key milestones and turning points that have shaped the study of AM (see, i.e. Fig.1). To this end, we briefly examine two closely related themes: (i) the interplay between electronic liquid crystal (ELC) phases<sup>12</sup>, multipole expansions<sup>13</sup>, and the emergence of the altermagnetism framework<sup>1,4,5</sup>; and (ii) the unconventional superconducting phenomena that naturally stem from this foundational interplay.

We begin by disentangling the similarities and differences among ELC phases, multipole expansions, and AM. Despite their distinct origins, all three share a common feature: spin-momentum locking (SML) at the nonrelativistic limit (as shown by the center Fig.1), although each is expressed in a different basis. In ELC phase, a single-band description suffices<sup>12</sup>. This single-band picture is also shared by the language of multipole expansions<sup>13</sup>, which offer a unified scheme for classifying ELC phases across all the charge and spin  $F_l^{S/A}$  (defined below) channels. Moreover, multipole expansions can be systematically extended to multisite systems, enabling a nature description of diverse magnetic textures, including collinear, coplanar, and noncoplanar magnets<sup>14</sup>. These magnetic textures, when classified at the nonrelativistic limit, fall within the framework of spin space groups<sup>15</sup>. Among them, AMs—a special type of collinear antiferromagnets (AFMs)—have attracted particular attention

in modern spintronics<sup>4</sup>. By integrating the advantages of both ferromagnets (FMs) and Néel antiferromagnets, AMs open a fertile arena for research, with rapid developments in recent years. Importantly, SML in AMs requires at least two sublattices with localized spins, meaning that a single-band description of SML in AMs should be understood as a low-energy effective approximation.

We then turn to the second theme: superconducting phenomena emerging from SML. The single-band description of SML provides a minimal yet powerful platform to explore unconventional superconductivity, an idea that has already been pursued within the context of ELC phases over the past few decades<sup>16</sup>. The emergence of AM has reignited this exploration, offering new opportunities to realize exotic pairing states rooted in SML. Yet, since single-band picture in AMs is only an approximation, we also highlight recent theoretical advances based on multisite models with localized spins in the discuss session, which point to richer possibilities for unconventional superconductivity in real materials.

This review is intended to serve both specialists and newcomers. For experts, it offers a conceptual consolidation of seemingly disparate ideas under a common framework; for a broader audience, it provides a heuristic introduction to the sequence of theoretical insights without dwelling on technical details. Our emphasis is on clarity of concepts rather than completeness of citations, and we direct readers to excellent existing reviews when discussing related topics in the following. We apologize in advance for any omissions in the literatures.

## II. A TALE OF THREE

High- $T_c$  cuprates<sup>17–19</sup> and  $f$ -electron systems<sup>20,21</sup> are two prototype strongly correlated systems. In cuprates,

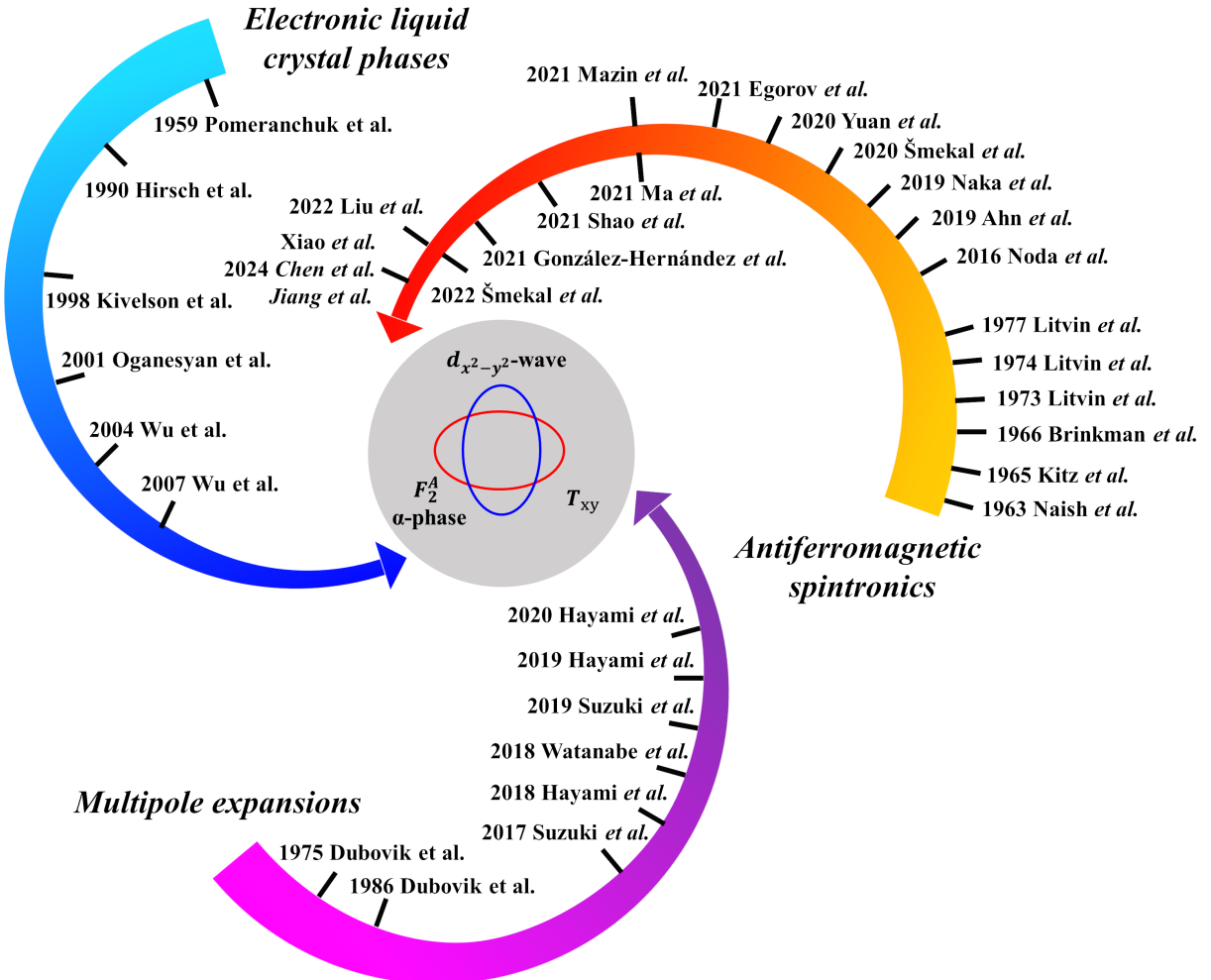


FIG. 1. A tale of three, where significant progress is chronologically displayed and labelled by year. While the idea of electronic liquid crystal phase is yet to be materialized, the multipole basis analysis of a collinear antiferromagnetic order with sublattices<sup>1</sup> and the symmetry classification based on spin-group theory<sup>4</sup> eventually lead to the discovery of altermagnetism.

the parent compounds are layered antiferromagnetic insulators. Upon electron or hole doping, the static antiferromagnetic order in CuO<sub>2</sub> plane gradually melts, simultaneously the insulating phase evolves into a metal, then *d*-wave superconductivity (SC) emerges. These intermediate "melted" phases, arising purely from electron-electron interactions, inspired the adoption of concepts in classical liquid crystals to classify the rich variety of electronic phases in cuprates and related materials<sup>16</sup>.

The *f*-electron systems, in contrast, are more naturally described through the framework of multipole expansions<sup>22,23</sup>. This distinction originates from the different character of *d* (the case in cuprates) and *f* electrons. The *d* electrons have much larger sensitivity to the crystal field produced by charges on neighboring ligands and a weaker spin-orbit coupling (SOC) when compared with *f* electrons. This usually leads to an almost complete quenching of the orbital degree of freedom of *d* electrons. Conversely, the interplay of spin and un-

quenched orbital degree of freedom in *f* electrons gives rise to a hierarchy of higher-rank multipoles beyond the familiar monopole and dipole. This has led to fruitful insights into ordering phenomena in *f*-electron systems. Not limited to *f*-electron systems, multipole basis has now been recognized as a unifying language for describing multipole degree of freedom of electrons in solids, e.g. charge, spin, and orbital, and many other properties (see reviews<sup>24,25</sup>).

Interestingly, the features of *d* electrons-sensitive to crystal field and weak SOC-can spur a very intriguing phenomenon: crystal-symmetry-protected spin splitting in collinear AFMs even without SOC. This unusual spin splitting facilitates the signal read-out in antiferromagnetic spintronics, therefore holds immense applications in energy-efficient quantum technologies. To capture the growing application list of such a phenomenon, a new class of collinear magnets-altermagnets-has recently been proposed, completing the traditional dichotomy of FMs

and AFMs. Today, AMs encompass both correlated metals and insulators, suggesting that their story is just beginning to unfold.

### A. Electronic liquid crystal phases

Electronic liquid crystal (ELC) phases are states of correlated quantum electronic systems that spontaneously break either rotational invariance or translational invariance<sup>16</sup>. Following the symmetry-based scheme used in classical liquid crystals<sup>26</sup>, there are four typical ELC phases: 1, crystalline phases which break all continuous translation and rotation symmetries; 2, smectic phases, which break one translation and/or rotation symmetry, exhibiting electron liquid behavior along the remaining symmetric direction. 3, nematic phases which break rotation symmetry while preserving translational symmetry, resulting in an anisotropic electron liquid with a preferred orientation axis, and 4, isotropic (liquid) phases, which preserve all symmetries, allowing electrons to flow uniformly in all directions. These ELC phases are characterized by long-range order parameters of charge, spin, orbital, and Cooper pair. Unlike their classical counterparts which are commonly melt by thermal fluctuations, ELC phases exhibit strong quantum mechanical effect, especially in the strongly correlation regime<sup>16</sup>, therefore they can be quantum melted at low temperatures, which gives quantum phase transitions.

Here, we focus primarily on the nematic phase of a Fermi liquid. This phase is characterized by electronic uniformity combined with directional anisotropy. There are two main pathways to reach the nematic phase: one involves a direct transition from the isotropic electronic fluid via a Pomeranchuk instability (PI)<sup>27</sup>, and the other occurs through the thermal or quantum melting a smectic phase<sup>16</sup>. In the following discussion, we concentrate on the former - the Pomeranchuk instability of Laudau Fermi liquid.

The central concept of the Laudau Fermi liquid theory is the existence of quasiparticles near the Fermi surface (FS) which weakly interact. Such interactions are parameterized by the Landau interaction functions  $F^{S/A}(\mathbf{k}, \mathbf{k}')$  quantifying the strength of the forward scattering amplitudes among quasiparticles at low energies with momenta  $\mathbf{k}, \mathbf{k}'$  close to the FS in the charge channel (superscript "S") or the spin channel (superscript "A"). If the system has translation symmetry, the Landau interaction functions only depends on the difference of the two momenta:  $F^{S/A}(\mathbf{k}, \mathbf{k}') = F^{S/A}(\mathbf{k} - \mathbf{k}')$ . Moreover, if the system conserve rotation symmetry, the Landau interaction functions can be decomposed into orthogonal angular momentum basis (or partial waves) and characterized by dimensionless Landau parameters. In 3D, spherical harmonics is a natural basis and the Landau parameters takes the form  $F_{l,m}^{S/A}$  where  $l$  ( $l \in \mathbb{N}$ ) and  $m$  ( $|m| \leq l$ ) is the azimuthal and magnetic quantum numbers. In 2D, circular harmonics is a natural basis and the

Landau parameters is simply  $F_l^{S/A}$ . For a lattice model, the continuous rotation symmetry is broken into discrete point group symmetry of the lattice, then the Landau parameters  $F_{l,m}^{S/A}/F_l^{S/A}$  are further split according to the irreducible representations (IRs) of the point group of the lattice.

The thermodynamic stability of the Fermi liquid state relies on the Pauli pressure from the Pauli exclusion principle. In 1958, Pomeranchuk<sup>27</sup> argued that if in one channel, the forward scattering interaction becomes sufficiently negative to overcome the stabilizing effects of the Pauli pressure, the Fermi liquid becomes unstable and undergoes distortion compatible with the symmetry of the unstable channel. Expressed in Landau parameters, we have the condition for PI:

$$\begin{aligned} F_{l,m}^{S/A} &\leq -(2l+1) \text{ in } 3D, \\ F_{l \neq 0}^{S/A} &\leq -2 \text{ in } 2D, \end{aligned} \quad (1)$$

We note that the  $l = 1$  and  $l = 2$  basis in 2D are  $\{x, y\}$  and  $\{2xy, x^2 - y^2\}$  in the real representation, and  $\{x \pm iy\}$  and  $\{(x \pm iy)^2\}$  in the complex representation.

In 2001, Oganesyan *et al.*<sup>28</sup> firstly studied the PI in the  $F_2^S$  channel (charge nematic state) with continuum models. Using a 2D single-band *spinless* system, they introduced the quadrupole density operator as a symmetric traceless tensor

$$\hat{\mathbf{Q}}(\mathbf{r}) \equiv -\frac{1}{k_F^2} \Psi^\dagger(\mathbf{r}) \begin{pmatrix} \partial_x^2 - \partial_y^2 & 2\partial_x\partial_y \\ 2\partial_x\partial_y & \partial_y^2 - \partial_x^2 \end{pmatrix} \Psi(\mathbf{r}) \quad (2)$$

where  $k_F$  is the Fermi wave vector. Such a tensor is equivalent to a complex operator  $\hat{Q}_2(\mathbf{r}) \equiv -\frac{1}{k_F^2} \Psi^\dagger(\mathbf{r})(\partial_x + i\partial_y)^2 \Psi(\mathbf{r})$  (where the subscript "2" represent the angular momentum  $l = 2$ ).

To obtain nonvanishing  $\mathbf{Q} \equiv \langle \hat{\mathbf{Q}}(\mathbf{r}) \rangle$ , Oganesyan *et al.* considered the following model Hamiltonian:

$$\begin{aligned} H = & \int d\mathbf{r} \Psi^\dagger(\mathbf{r}) \epsilon(\vec{\nabla}) \Psi(\mathbf{r}) \\ & + \frac{1}{4} \int d\mathbf{r} \int d\mathbf{r}' F_2(\mathbf{r} - \mathbf{r}') \text{Tr}[\hat{\mathbf{Q}}(\mathbf{r}) \hat{\mathbf{Q}}(\mathbf{r}')] \end{aligned} \quad (3)$$

where the free-fermion dispersion (near the FS) is  $\epsilon(\mathbf{k}) = v_F q [1 + a(q/k_F)^2]$  with  $v_F$  the Fermi velocity and  $q \equiv |\mathbf{k}| - k_F$ , and the interparticle interaction is given in the form  $F_2(\mathbf{r}) = \frac{1}{(2\pi)^2} \int d\mathbf{q} e^{i\mathbf{q}\mathbf{r}} \frac{F_2}{1 + \kappa F_2 q^2}$ , where  $F_2$  is an appropriate parameter related to the  $l = 2$  Landau parameter  $F_2^S$ , and  $\kappa$  measures the range of the two-body interactions.

By utilizing a Hubbard-Stratonovich decoupling, the Landau energy density functional for this model can be written as<sup>28</sup>:

$$F[\mathbf{Q}] = E[\mathbf{Q}] - \frac{\tilde{\kappa}}{4} \text{Tr}[\mathbf{Q} \mathbf{D} \mathbf{Q}] - \frac{\tilde{\kappa}'}{4} \text{Tr}[\mathbf{Q}^2 \mathbf{D} \mathbf{Q}] + \dots \quad (4)$$

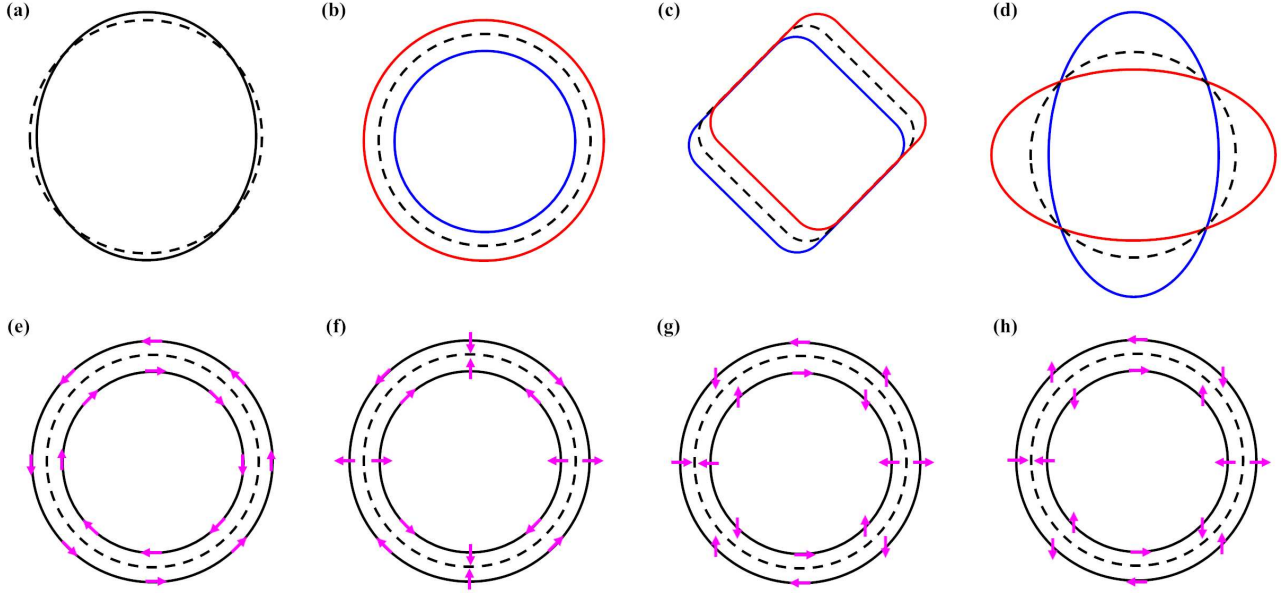


FIG. 2. Fermi surfaces of different electronic liquid crystal phases. (a) charge nematic state, (b) itinerant FM state, (c)  $l = 1$  or  $p$ -wave  $\alpha$  state, (d)  $l = 2$  or  $d$ -wave  $\alpha$  state, which bears similarity to the  $d$ -wave AM, (e)-(h) various  $\beta$  phases. The dashed line denotes the isotropic Fermi surfaces.

where  $D_{i,j} \equiv \partial_i \partial_j$ , and  $\tilde{\kappa}$  and  $\tilde{\kappa}'$  are the two effective Franck constants. The uniform part of the energy functional  $E[\mathbf{Q}]$  is given by

$$E[\mathbf{Q}] = E(0) + \frac{A}{4} \text{Tr}[\mathbf{Q}^2] + \frac{B}{8} \text{Tr}[\mathbf{Q}^4] + \dots \quad (5)$$

where  $A = 1/(2N_F) + F_2$  with  $N_F$  the density of state at the FS, and  $B = (3aN_F|F_2|^3)/(8v_F^2 k_f^2)$ . The isotropic Fermi liquid phase becomes unstable provided  $A < 0$ , or equivalently,  $2N_F F_2 < -1$ , which is the PI condition in this spinless model. The result of such an instability is a spontaneously distorted FS characterized by the nonzero order parameter  $\mathbf{Q}$  (see Fig.2(a)), which has the name nematic phase in analogy to classical electronic liquid phase. Results on lattice models can be found in Kee *et al.*<sup>29</sup>, Khavkine *et al.*<sup>30</sup>, Yamase *et al.*<sup>31</sup>, Lamas *et al.*<sup>32</sup>, Quintanilla *et al.*<sup>33</sup>.

Now we discuss the spin channel ( $F_l^A$ ), which is more relevant. The simplest case is the  $l = 0$  channel, the PI  $F_0^A < -1$  gives just the well-known Stoner criterion  $N_F U > 1$  for itinerant FMs<sup>34</sup>, if we consider the Hubbard model with on-site Hubbard interaction strength  $U$ . Obviously, the spatial inversion ( $\mathcal{P}$ ) and rotation symmetries are conserved but time reversal ( $\mathcal{T}$ ) invariance is broken in this channel, as shown in Fig.2(b).

In 1990, Hirsch *et al.*<sup>35</sup> first proposed a spin-split state, i.e. a  $F_1^A$  channel PI, by considering the following Hamiltonian:

$$\hat{H} = \sum_{\langle i,j \rangle} \sum_{\sigma} (\hat{c}_{i\sigma}^\dagger \hat{c}_{j\sigma} + h.c.) + J \hat{c}_{i\sigma}^\dagger \hat{c}_{j\sigma} \hat{c}_{j\bar{\sigma}}^\dagger \hat{c}_{i\bar{\sigma}}, J > 0 \quad (6)$$

Actually the second term just gives the XY-model  $\sum_{\langle i,j \rangle} -J(\hat{S}_i^+ \hat{S}_j^- + \hat{S}_i^- \hat{S}_j^+)$ . Such a model hosts three

phases: paramagnetic phase preserving both  $\mathcal{P}$  and  $\mathcal{T}$ , ferromagnetic phase preserving  $\mathcal{P}$  but breaking  $\mathcal{T}$ , and spin-split state preserving  $\mathcal{T}$  but breaking  $\mathcal{P}$ . For a 2D square lattice near half-filling, such a spin-split state is shown in Fig.2(c), where the spin-up and spin-down FSs shift along opposite direction without changing the number of spin-up and spin-down electrons. In 2006, Varma *et al.*<sup>36</sup> considered a continuum model in 3D and obtained a similar spectrum shown in Fig.2(c), such states are called helicity-ordered states, which is believed to be the "hidden order parameter" in  $\text{URu}_2\text{Si}_2$ <sup>37,38</sup>.

A systematic investigation of  $F_l^A$  channel PI was laid out by Wu *et al.*<sup>12,39</sup>, generalizing the earlier idea by Oganesyan *et al.*<sup>28</sup> to the spin channel. Wu *et al.*<sup>12,39</sup> discussed both 2D and 3D cases. Here, for simplicity we focus on the 2D case. In 2D, the multipole spin density operator in complex representation is given by:

$$\hat{Q}_l^a = \sum_{\alpha\beta} \Psi_\alpha^\dagger(\mathbf{r}) \sigma_{\alpha\beta}^a (\partial_x + i\partial_y)^l \Psi(\mathbf{r})_\beta \quad (7)$$

where  $\sigma^a (a = x, y, z)$  represent the three Pauli matrices. The order parameter  $Q_l^a \equiv \langle \hat{Q}_l^a \rangle$  obeys the following transformation laws: (1)  $\mathcal{P} Q_l^a \mathcal{P}^{-1} = (-1)^l Q_l^a$ ; (2)  $\mathcal{T} Q_l^a \mathcal{T}^{-1} = (-1)^{l+1} Q_l^a$ ; and (3)  $Q_l^a$  is invariant under a rotation by  $\pi/l$  followed by a spin flip. The first two properties indicate that  $Q_l^a$  are actually electronic and magnetic toroidal multipoles for odd and even  $l$  (see Tab.I and the related discussions in the next subsection). The third transformation law, under a combined effect of independent spatial and spin rotations, is a key property of spin group<sup>15</sup>, which plays an important role in AM, as we shall see.

The order parameter  $Q_l^a$  can be decomposed into the real and complex part,  $Q_l^a \equiv n_1^a + i n_2^a$  and hence can be represented by two vectors  $\mathbf{n}_1 = (n_1^x, n_1^y, n_1^z)$  and  $\mathbf{n}_2 = (n_2^x, n_2^y, n_2^z)$ . Wu *et al.*<sup>12,39</sup> have shown that the Landau-Ginzburg free energys takes the form:

$$F[\mathbf{n}_1, \mathbf{n}_1] = r(\mathbf{n}_1^2 + \mathbf{n}_2^2) + v_1(\mathbf{n}_1^2 + \mathbf{n}_2^2)^2 + v_2|\mathbf{n}_1 \times \mathbf{n}_2|^2 \quad (8)$$

where  $r$ ,  $v_1$ , and  $v_2$  are three parameters (or coupling constants) to be determined by the microscopic model Hamiltonian. The PI occurs at  $r < 0$  for  $F_l^A < -2$ . There are two symmetry broken phases: (1) if  $v_2 > 0$ , then  $\mathbf{n}_1 \parallel \mathbf{n}_2$ . This is dubbed as "α" phase, a name comes from the  $A$  phase in liquid  $^3\text{He}$ . In the  $\alpha$  phase, the spin-up and spin-down FSs are distorted but are rotated from each other by  $\pi/l$ . The spin-split state (see Fig.2(c)) proposed by Hirsch *et al.* and the helicity-ordered state proposed by Varma *et al.* are the  $l = 1 \alpha$  phase. Fig.2(d) shows the  $l = 2 \alpha$  phase. This is also the "nematic-spin-nematic" state discussed briefly by Kivelson *et al.* in 2003<sup>40</sup>. (2) If  $v_2 < 0$ , then  $\mathbf{n}_1 \perp \mathbf{n}_2$  and  $|\mathbf{n}_1| = |\mathbf{n}_2|$ . This is dubbed as "β" phases, in analogy to the  $B$  phase in liquid  $^3\text{He}$ . In the  $\beta$  phases, the FSs split into two parts with different areas, while each one keeps the circle shape as shown in Fig.2(e)-(h). The spin texture in  $\beta$  phase exhibit the vortex structure in  $\mathbf{k}$  space, so spin is no longer a good quantum number. To see the spin texture, Wu *et al.* defined the  $\mathbf{d}$  vector<sup>12</sup>

$$\mathbf{d}(\mathbf{k}) = (\cos(l\theta_{\mathbf{k}}), \sin(l\theta_{\mathbf{k}})) \quad (9)$$

where  $\theta_{\mathbf{k}}$  is the azimuthal angle of  $\mathbf{k}$  in the 2D plane. For the same  $l$ , there are two different spin configurations characterized by opposite winding numbers. For example, Fig.2(e)-(f) both have  $l = 1$ , but the spin circulates counterclockwisely when enclosing the outer FS in Fig.2(e), clockwise in Fig.2(f). The same applies for Fig.2(g)-(h). The spin texture in Fig.2(e) and Fig.2(f) are the well-known Rashba-type SOC and Dresselhaus-type SOC, but Fig.2(g) and Fig.2(h) are totally undiscovered<sup>39</sup>.

Based on the above analysis, Wu<sup>41</sup> termed the  $F_l^A (l > 0)$  channel PI as "unconventional magnetism", a name following the spirit of unconventional superconductivity to emphasize the non-trivial representations of the rotation group. Although the term "magnetism" appears in this definition, it should be noted that there can be no localized magnetic moments in unconventional magnetism. Unconventional magnetism under magnetic dipolar interactions, which is a form of SOC, can be found in Fu *et al.*<sup>42</sup>, Norman *et al.*<sup>43</sup>, and Yuan *et al.*<sup>44</sup>.

From above classification, it is readily seen that to identify an ELC phase, four types of indexes are required: the channel index  $l$  and the charge/spin index of the Landau parameter  $F_l^A$ , the  $\alpha$  or  $\beta$  phase for isotropic or anisotropic FSs, and a winding number to distinguish the spin texture at the same  $l$ . In the framework of multipole basis, we will see that these four indexes will be unified.

## B. Multipole expansions

Textbooks in classical electrodynamics introduce two types of multipoles, electric (**E**) and magnetic (**M**) multipoles<sup>45</sup>. In 1975, Dubovik *et al.*<sup>46</sup> discovered the magnetic toroidal (**MT**) multipoles "hidden" in the classical Maxwell's equation. In condensed matter physics, **MT** multipoles have been extensively investigated owing to its potential role in exotic phenomena. Interested readers can refer to reviews<sup>47,48</sup>.

It seems that there should only be three multipoles **E**, **M**, and **MT** in nature. However, they are insufficient to form a complete vector basis of multipole representations under  $\mathcal{P}$  and  $\mathcal{T}$ . Therefore, in 1986 Dubovik *et al.*<sup>49</sup> introduced a forth multipole called electric toroidal (**ET**) multipole. A phenomenological introduction about this history is given by Nanz *et al.*<sup>50</sup>. **E**, **M**, **MT**, and **ET** transform as a polar tensor with time-reversal even, axial tensor with time-reversal odd, polar tensor with time-reversal odd, and axial tensor with time-reversal even, therefore exhausting all possibilities under  $\mathcal{P}$  and  $\mathcal{T}$ . Under rotational symmetry, **E**, **M**, **MT**, and **ET** can be represented in different partial waves as  $Q_{lm}$ ,  $M_{lm}$ ,  $G_{lm}$ , and  $T_{lm}$  in 3D. The transformation property of  $Q_{lm}$ ,  $M_{lm}$ ,  $G_{lm}$ , and  $T_{lm}$  multipoles under  $\mathcal{P}$  and  $\mathcal{T}$  is shown in Tab.I. From the table, it is clear that the order parameter  $Q_l^a$  defined in Eq.7 is actually **E** multipole for odd  $l$  and **MT** multipole for even  $l$ .

The concept of multipole expansions is also applied to describe atomic-scale electromagnetic distribution of the wave-function of electrons bound to a single-centered atom, leading to the so called atomic multipole basis. Such a terminology emphasizes that the multipoles form a complete basis set and each multipole basis is equally important for describing physical properties, to be distinguished from the conventional multipole expansion where higher-order multipoles are less important and contribute only weakly. Due to the highly localized  $f$  electrons, multipole basis has a long history in studying  $f$ -electron systems, especially the "hidden order" whose order parameters are hard to identify. For more details, we refer to the excellent review articles<sup>22,23</sup>.

Although the expressions of quantum operators for **E** and **M** multipole have been known during the ongoing explorations of  $f$ -electron system, the expressions for **MT** and **ET** multipoles are known only recently by Hayami *et al.* in 2018<sup>51</sup>. For a single-band model, these operators

TABLE I. Transformation properties of  $Q_{lm}$ ,  $M_{lm}$ ,  $G_{lm}$ , and  $T_{lm}$  multipoles under  $\mathcal{P}$  and  $\mathcal{T}$ .

Multipole types	Multipole symbol	$\mathcal{P}$	$\mathcal{T}$
<b>E</b>	$Q_{lm}$	$(-1)^l$	+
<b>M</b>	$M_{lm}$	$(-1)^{l+1}$	-
<b>MT</b>	$G_{lm}$	$(-1)^l$	-
<b>ET</b>	$T_{lm}$	$(-1)^{l+1}$	+

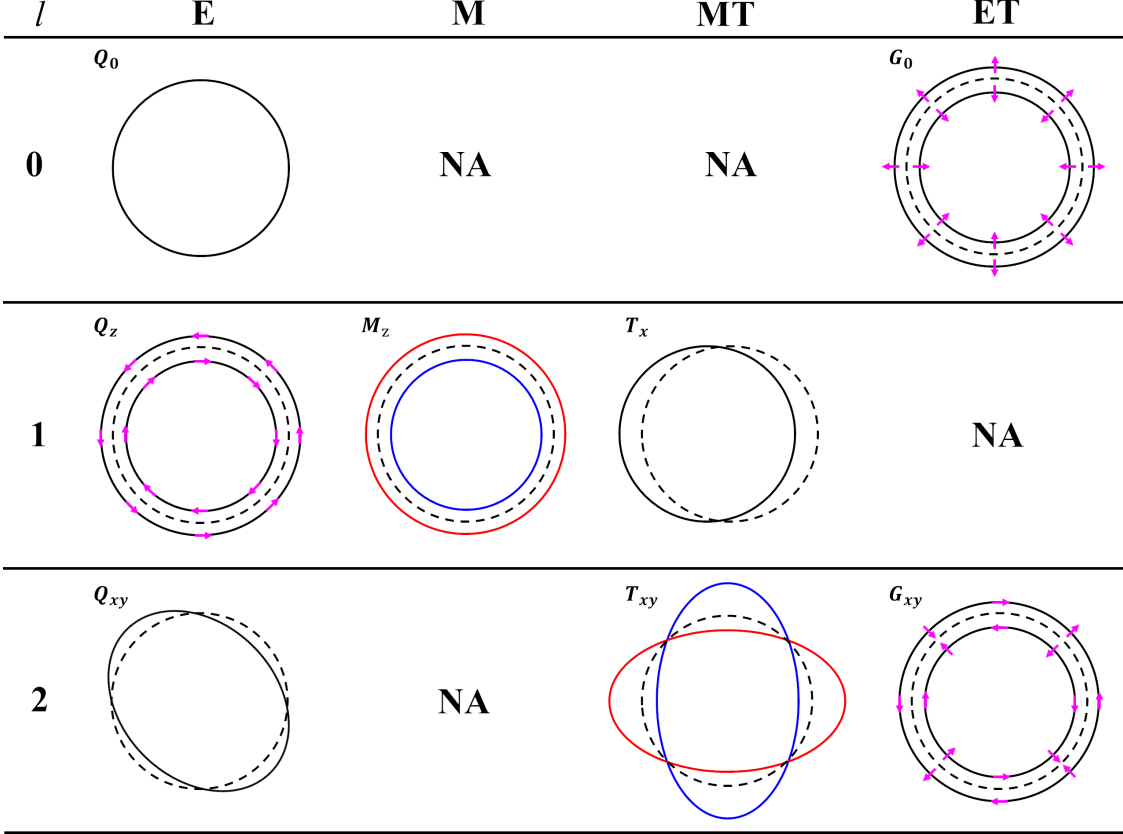


FIG. 3. Multipole basis up to  $l = 2$ . The dashed line denotes the Fermi surfaces with vanishing multipoles. "NA" means not allowed by symmetry. It is useful to compare the various phases in this figure with the ones in Fig.2. In particular, the dispersion relation of the **MT** quadrupole  $T_{xy}$  should be contrasted with that of  $F_2^A$   $\alpha$ -phase shown in Fig.2(d), both of which exhibit a similar feature as the  $d$ -wave AM.

in  $\mathbf{k}$  space are given by<sup>13</sup>:

$$Q_{lm}(\mathbf{k}) \equiv \begin{cases} \sigma_0 O_{lm}(\mathbf{k}) & (l = 0, 2, 4, 6, \dots) \\ (\mathbf{k} \times \boldsymbol{\sigma}) \cdot \nabla_{\mathbf{k}} O_{lm}(\mathbf{k}) & (l = 1, 3, 5, \dots) \end{cases}, \quad (10a)$$

$$M_{lm}(\mathbf{k}) \equiv \begin{cases} 0 & (l = 0, 2, 4, 6, \dots) \\ \boldsymbol{\sigma} \cdot \nabla_{\mathbf{k}} O_{lm}(\mathbf{k}) & (l = 1, 3, 5, \dots) \end{cases}, \quad (10b)$$

$$T_{lm}(\mathbf{k}) \equiv \begin{cases} 0 & (l = 0) \\ (\mathbf{k} \times \boldsymbol{\sigma}) \cdot \nabla_{\mathbf{k}} O_{lm}(\mathbf{k}) & (l = 2, 4, 6, \dots) \\ \sigma_0 O_{lm}(\mathbf{k}) & (l = 1, 3, 5, \dots) \end{cases}, \quad (10c)$$

$$G_{lm}(\mathbf{k}) \equiv \begin{cases} \mathbf{k} \cdot \boldsymbol{\sigma} & (l = 0) \\ \boldsymbol{\sigma} \cdot \nabla_{\mathbf{k}} O_{lm}(\mathbf{k}) & (l = 2, 4, 6, \dots) \\ 0 & (l = 1, 3, 5, \dots) \end{cases}, \quad (10d)$$

where  $\boldsymbol{\sigma} = (\sigma^x, \sigma^y, \sigma^z)$  and the harmonics  $O_{lm}(\mathbf{k})$  is defined as

$$O_{lm}(\mathbf{k}) = \sqrt{\frac{4\pi}{2l+1}} k^l Y_{lm}^*(\hat{\mathbf{k}}) \quad (11)$$

with  $Y_{lm}(\hat{\mathbf{k}})$  the spherical harmonics of the angles  $\hat{\mathbf{k}} = \mathbf{k}/k$ . To make a specific connection with the previous section, we note that the electric quadrupole  $O_{22}(\mathbf{k}) = (k_x + ik_y)^2$ . In the second quantization, it takes the form  $\Psi^\dagger(\mathbf{r})(\partial_x + i\partial_y)^2\Psi(\mathbf{r})$ , which is an equivalent representation of Eq.2.

The one-electron Hamiltonian is a  $\mathcal{P}$  and  $\mathcal{T}$  invariant scalar<sup>13</sup>:

$$\mathcal{H} = \sum_{X}^{Q,M,T,G} \sum_{\mathbf{k}\alpha\beta} \sum_{lm} X_{lm}^{ext} X_{lm}^{\alpha\beta}(\mathbf{k}) \hat{c}_{\mathbf{k}\alpha}^\dagger \hat{c}_{\mathbf{k}\beta} \quad (12)$$

where  $\hat{c}_{\mathbf{k}\alpha}^\dagger$  ( $\hat{c}_{\mathbf{k}\alpha}$ ) is the creation (annihilation) operator of an electron with the wave vector  $\mathbf{k}$  and spin  $\alpha$ . Here we have assume  $X_{lm}$  in real representation (which can be achieved by taking linear combination of  $X_{lm}$ ) so that the Hermite conjugation is omitted in the scalar product.  $X_{lm}^{ext}$  represent "symmetry breaking" fields (also known as conjugate fields), which cause symmetry-breaking for certain multipoles. In order to examine the effect of multipoles on the band structure, in the single-band systems,

the Hamiltonian in Eq.12 can be divided as

$$\mathcal{H} = \sum_{\mathbf{k}\alpha\beta} [\varepsilon^E(\mathbf{k})\delta_{\alpha\beta} + \varepsilon^O(\mathbf{k})\delta_{\alpha\beta} + f_{\alpha\beta}^E(\mathbf{k}) + f_{\alpha\beta}^O(\mathbf{k})] \hat{c}_{\mathbf{k}\alpha}^\dagger \hat{c}_{\mathbf{k}\beta} \quad (13)$$

where  $\varepsilon$  ( $f_{\alpha\beta}$ ) denotes the charge (spin) sector and the superscript  $E(O)$  represents symmetric (antisymmetric) contribution with respect to  $\mathbf{k}$ . As the even-rank  $Q_{lm}(\mathbf{k})$ ,  $T_{lm}(\mathbf{k})$ , and the odd-rank  $M_{lm}(\mathbf{k})$  are even function of  $\mathbf{k}$ , and other multipoles are odd function of  $\mathbf{k}$ , each coefficient in Eq.13 is identified as:

$$\varepsilon^E(\mathbf{k}) = \sum_{lm}^{even} Q_{lm}^{ext} Q_{lm}(\mathbf{k}), \quad (14a)$$

$$\varepsilon^O(\mathbf{k}) = \sum_{lm}^{odd} T_{lm}^{ext} T_{lm}(\mathbf{k}), \quad (14b)$$

$$f_{\alpha\beta}^E(\mathbf{k}) = \sum_{lm}^{odd} M_{lm}^{ext} M_{lm}^{\alpha\beta}(\mathbf{k}) + \sum_{lm}^{even} T_{lm}^{ext} T_{lm}^{\alpha\beta}(\mathbf{k}), \quad (14c)$$

$$f_{\alpha\beta}^O(\mathbf{k}) = \sum_{lm}^{odd} Q_{lm}^{ext} Q_{lm}^{\alpha\beta}(\mathbf{k}) + \sum_{lm}^{even} G_{lm}^{ext} G_{lm}^{\alpha\beta}(\mathbf{k}). \quad (14d)$$

By diagonalizing Eq.13 with  $X_{lm}^{ext}$  working as constants, we can obtain different types of band structures. In the following, typical cases are discussed and are contrasted with the 2D results of the  $F_l^{S/A}$  channels in the previous subsection:

i)  $\varepsilon^E(\mathbf{k})$  in Eq.14a represents a symmetric band dispersion without spin splitting. This band structure is present when both  $\mathcal{P}$  and  $\mathcal{T}$  exist. The **E** monopole gives the kinetic energy of free electron  $\varepsilon(\mathbf{k}) \propto Q_0^{ext}\mathbf{k}^2$ . This is shown in the first row (i.e.,  $l = 0$ ) and first column (i.e., the column **E**) of Fig.3. The **E** quadrupole  $Q_{xy}$ , accompanying the **E** monopole, gives the band dispersion  $\varepsilon(\mathbf{k}) \propto Q_0^{ext}\mathbf{k}^2 + Q_{xy}^{ext}k_x k_y$  which describes an ellipse as shown in the third row and first column of Fig.3. This quadrupole-type deformation corresponds to the orbital nematic order  $F_2^S$  described by Oganesyan *et al.*<sup>28</sup> (see Fig.2(a)).

ii)  $\varepsilon^O(\mathbf{k})$  in Eq.14b represents the asymmetric-type band dispersions with spin degeneracy. For example, the **MT** dipole  $T_x$ , accompanying the **E** monopole, leads to a shift along  $k_x$  direction in the dispersion relation  $\varepsilon(\mathbf{k}) \propto Q_0^{ext}\mathbf{k}^2 + T_x^{ext}k_x$ , as shown in the second row and third column of Fig.3. Obviously, this band structure occurs when both  $\mathcal{P}$  and  $\mathcal{T}$  are broken. Actually it corresponds to the  $F_1^S$  channel instability.

iii)  $f_{\alpha\beta}^E(\mathbf{k})$  in Eq.14c represents a symmetric-type band dispersion with spin splitting, which appears for system with conserved  $\mathcal{P}$  but broken  $\mathcal{T}$ . The simplest case is considering the **M** monopole  $M_z$ , accompanying the **E** monopole, gives the band dispersion  $\varepsilon_\sigma(\mathbf{k}) \propto Q_0^{ext}\mathbf{k}^2 + M_z^{ext}\sigma$  with  $\sigma = \pm 1$ . With  $M_z^{ext}$  contributed by either Weiss molecular field of the spontaneous ferromagnetic ordering or an external field, this give an isotropic spin splitting as shown in the second row and second

column of Fig.3, corresponding to the  $F_0^A$  channel PI. Another non-trivial case is the **MT** quadrupole  $T_{xy}$ , accompanying the **E** monopole, which leads to the band dispersion  $\varepsilon_\sigma(\mathbf{k}) \propto Q_0^{ext}\mathbf{k}^2 + \sigma T_{xy}^{ext}(k_x^2 - k_y^2)$  (where we have set  $k_z = 0$  for simplicity). This is an anisotropic spin splitting as shown in the third row and third column of Fig.3, corresponding to the  $F_2^A$  channel PI in the  $\alpha$  phase, or corresponding to the spin splitting in the  $d_{x^2-y^2}$ -wave AM, as we shall see.

iv)  $f_{\alpha\beta}^O(\mathbf{k})$  in Eq.14d represents the asymmetric-type band dispersion with spin splitting. For example, the **E** dipole  $Q_z$  gives the Rashba-type SOC  $k_y\sigma_x - k_x\sigma_y$ , and the **E** octupole  $Q_{xyz}$  gives the Dresselhuas-type SOC  $k_x(k_y^2 - k_z^2)\sigma_x + k_y(k_z^2 - k_x^2)\sigma_y + k_z(k_x^2 - k_y^2)\sigma_z$ . In 2D, the **E** dipole  $Q_x$  becomes  $k_y\sigma_z$ , accompanying **E** monopole, gives the band dispersion  $\varepsilon_\sigma(\mathbf{k}) = Q_0^{ext}\mathbf{k}^2 + \sigma Q_x^{ext}k_y$ , which gives the spin-split state in Fig.2(c). The **ET** monopole  $G_0$  gives the hedgehog-type SOC  $\mathbf{k} \cdot \boldsymbol{\sigma}$ , and the **ET** quadrupole  $G_{xy}$  gives the SOC  $k_x\sigma_y + k_y\sigma_x$ .

From the above discussion, we can readily see that multipole basis can be understood as a unified description of the charge and spin channel PI for a single-band model Hamiltonian.

Multipole basis can also be employed to describe magnetic structures which will be discussed in the following subsection. To achieve this, it is necessary to generalize single-site multipoles to multi-site systems, just as the way cluster orbitals are introduced on the top of atomic orbitals. In 2017, Suzuki *et al.*<sup>52</sup> introduced the concept of cluster multipoles to provide a unified framework for describing the intrinsic anomalous Hall effect (AHE) in magnetic materials. By taking linear combination of atomic **M** multipoles at symmetry-equivalent Wyckoff positions, they constructed cluster **M** multipoles, which can be further classified according to the point group symmetry of the cluster. This type of multipole expansions now is referred to as the symmetry-adapted multipole basis (SAMB)<sup>24</sup>. Suzuki *et al.* demonstrated that a necessary condition for the AHE is a nonvanishing **M** SAMB that transforms like a magnetic dipole moment<sup>52</sup>. Since **M** and **MT** multipoles are odd under  $\mathcal{T}$ , their corresponding SAMBs can be used to construct arbitrary magnetic structures<sup>53</sup>. In other words, multi-site multipole basis provide an alternative method to scrutinize spin space group (see, i.e., the next subsection). Furthermore, the two polar **E** and **MT** SAMBs can be used to describe SML in AFMs<sup>1,14,54</sup>.

### C. Altermagnetism

AFM could represent next-generation spintronic applications<sup>55,56</sup>, owing to their unique combination of properties: i) they are inherently robust against perturbation against external magnetic field disturbances; ii) they generate zero stray fields, allowing for high-density device integration; and iii) they exhibit ultrafast dynamics reaching the terahertz range, enabling exceptionally

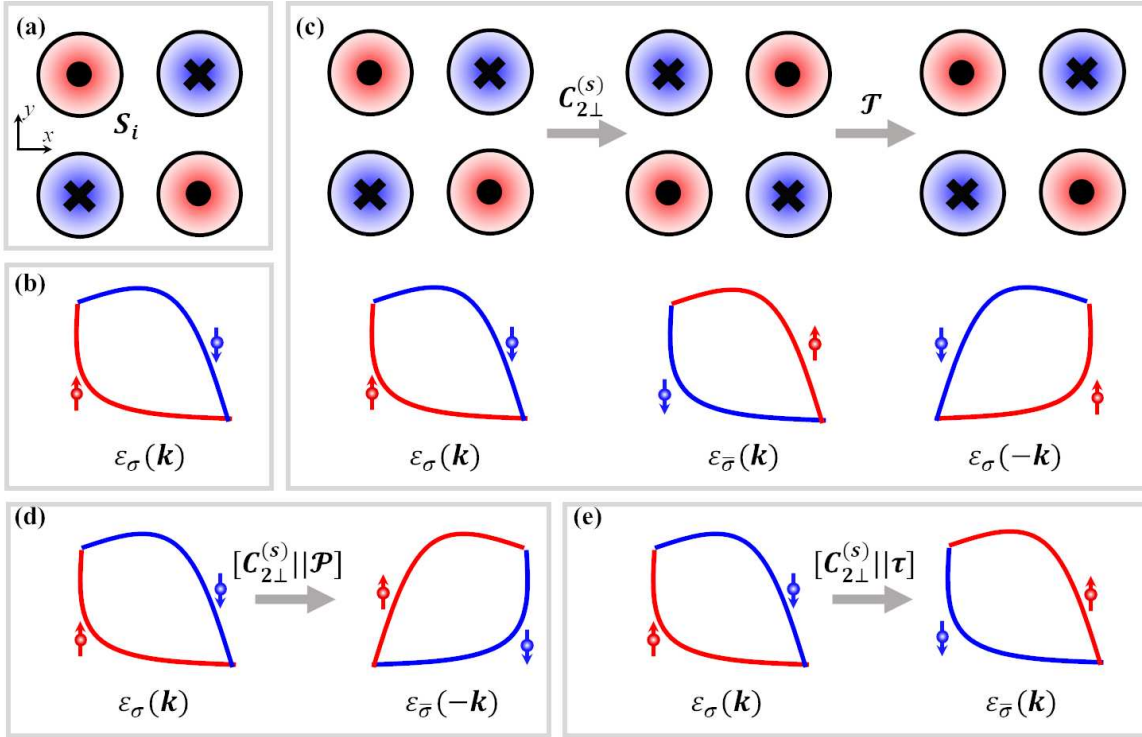


FIG. 4. (a) Schematic representation of a collinear magnet, here the local magnetic moment  $S_i$  is perpendicular to the paper plane ( $xoy$  plane). (b) Spin-polarized band structure of collinear magnets. (c) Top: both  $C_{2\perp}^{(s)}$  and  $\mathcal{T}$  flips local magnetic moment  $S_i$  in real space. Bottom: the combination of  $C_{2\perp}^{(s)}$  and  $\mathcal{T}$  functions as  $\mathcal{P}$  for the energy spectrum. (d)  $[C_{2\perp}^{(s)} || \mathcal{P}]$  works as  $\mathcal{T}$  for the energy spectrum. (e)  $[C_{2\perp}^{(s)} || \tau]$  protects spin degeneracy.

high-speed response. However, the absence of net magnetization in AFM poses a significant challenge for signal readout, as traditional electromagnetic methods do not couple with the AFM order parameter.

The discovery of the AHE in the noncollinear AFM  $Mn_3Sn^{57}$  has partially addressed the signal readout challenge in AFM systems. This breakthrough has lead to the emergence of a new subfield known as noncollinear AFM spintronics (see reviews<sup>58,59</sup>). However, the intricate magnetic texture inherent to noncollinear AFMs can lead to rapid decoherence of spin excitations. This limitation has driven interest in *collinear* AFM spintronics, where the focus is on achieving longer spin coherence lengths.

### 1. Symmetry aspects of collinear AFMs

Collinear magnets possess two intrinsic on-site symmetries, regardless of their specific magnetic configuration<sup>4,15</sup>. For a collinear magnet illustrated in Fig.4(a), all local magnetic moments  $S_i$  at site "i" are aligned perpendicular to the paper plane, i.e. along the  $z$ -direction. Because the spin configuration remains invariant under arbitrary spin rotations about the  $z$ -axis, thus collinear magnet exhibit a  $U_s(1)$  symmetry, where the subscript "s" highlights that the rotation occurs in spin

space. As a result, spin remains a good quantum number, and each Bloch state maintains a definite spin projection of  $\pm\frac{1}{2}$ , as shown by the red/blue color in Fig.4(b). In addition to this continuous spin rotational symmetry, collinear magnets also exhibit a second discrete symmetry, shown in Fig.4(c): a  $180^\circ$  spin rotation about an axis perpendicular to the  $z$ -axis (denoted as  $C_{2\perp}^{(s)}$ ), followed by the time reversal operation  $\mathcal{T}$ . This combined operation is formally denoted as  $[C_{2\perp}^{(s)} || \mathcal{T}]$ , where in general the transformation on the left and right sides of the double vertical bar acts in spin space and in real space, respectively. Such a symmetry imposes the constraint  $\varepsilon_\sigma(\mathbf{k}) = \varepsilon_{\bar{\sigma}}(-\mathbf{k})$  on the band structure. While the system may lack real-space inversion symmetry  $\mathcal{P}$ , this combined spin-space symmetry effectively plays the role of  $\mathcal{P}$  in determining the energy spectrum. For more discussions, we refer to Appendix A and Appendix B of the pioneering work on spin groups<sup>15</sup>.

At this point, it is helpful to clarify why conventional AFMs typically exhibit Kramers degeneracy  $\varepsilon_\sigma(\mathbf{k}) = \varepsilon_{\bar{\sigma}}(\mathbf{k})$ . This spin degeneracy arises from two fundamental symmetries<sup>4</sup>. The first one is  $C_{2\perp}^{(s)}$  followed by  $\mathcal{P}$  as shown in Fig.4(d). Together, this combined symmetry effectively mimic time-reversal symmetry  $\mathcal{T}$ , as the Bloch state now satisfies  $\varepsilon_\sigma(\mathbf{k}) = \varepsilon_{\bar{\sigma}}(-\mathbf{k})$ . Since collinear AFMs inherently posses an effective  $\mathcal{P}$  as we just mentioned, the

existence of both effective  $\mathcal{P}$  and effective  $\mathcal{T}$  guarantees that each Bloch state is doubly degenerated. The second symmetry involves the same  $C_{2\perp}^{(s)}$  spin rotation, but followed by a fractional lattice translation  $\tau$ , connecting the two magnetic sublattices. While  $\tau$  introduces only a phase factor to the Bloch state without changing the energy spectrum, this combined symmetry operation leads to Kramers degeneracy as shown in Fig.4(e).

## 2, Prelude to altermagnetism

Breaking Kramers degeneracy, even just over a small portion of the first Brillouin zone (FBZ), provides the first step toward collinear AFM spintronics. First-principles calculations have played important roles in searching for lifted Kramers degeneracy in collinear AFM. By employing DFT+U calculation for different MnO<sub>2</sub> phases, Noda *et al.*<sup>60</sup> firstly reported SML in collinear AFM. It should be noted that before the work by Noda *et al.*<sup>60</sup>, Franchini *et al.*<sup>61</sup> have studied the ground state of  $\beta$ -MnO<sub>2</sub> and Cockayne *et al.*<sup>62</sup> have studied the ground state of  $\alpha$ -MnO<sub>2</sub>. However, no band structures are explicitly displayed in those studies.

Noda *et al.*<sup>60</sup> also demonstrated a symmetry analysis to unveil the spin splitting and spin degeneracy at a given  $\mathbf{k}$ -point in the FBZ. In the Kohn-Sham framework, the single-electron potential  $V_\sigma$  is spin dependent for a collinear magnet, so the Kohn-Sham equation for spin-up and spin-down electrons are:

$$[\frac{1}{2}(\mathbf{k} - i\vec{\nabla})^2 + V_\uparrow]u_\uparrow(\mathbf{k}) = \varepsilon_\uparrow(\mathbf{k})u_\uparrow(\mathbf{k}), \quad (15a)$$

$$[\frac{1}{2}(\mathbf{k} - i\vec{\nabla})^2 + V_\downarrow]u_\downarrow(\mathbf{k}) = \varepsilon_\downarrow(\mathbf{k})u_\downarrow(\mathbf{k}), \quad (15b)$$

where  $u_\sigma(\mathbf{k})$  denotes the periodic eigenfunctions at each  $\mathbf{k}$ . Now suppose a space-group operation  $\mathcal{R}$  that maps the single-electron potential as  $\mathcal{R}V_\sigma\mathcal{R}^{-1} = V_{\bar{\sigma}}$ . In the case that a certain wave vector  $\mathbf{k}$  is invariant under  $\mathcal{R}$ , i.e.  $\mathcal{R}\mathbf{k} = \mathbf{k}$ , the Hamiltonian of the spin-up and spin-down electron are exchanged under  $\mathcal{R}$ , which gives Kramers degeneracy  $\varepsilon_\uparrow(\mathbf{k}) = \varepsilon_\downarrow(\mathbf{k})$ . However, away from these high symmetric points, for general wave vectors  $\mathbf{k}$  and  $\mathbf{k}' = \mathcal{R}\mathbf{k}$ , then we have spin-momentum locking  $\varepsilon_\uparrow(\mathbf{k}) = \varepsilon_\downarrow(\mathbf{k}')$ .

It is also worth noting that Noda *et al.*<sup>60</sup> highlighted the critical role of oriented MnO<sub>6</sub> octahedron in modifying the magnetization densities around Mn atoms, leading to the emergence of a staggered potential  $V_\sigma$ . A common mechanism for introducing such oriented MO<sub>6</sub> octahedron in transition metal compounds is the Jahn-Teller distortion. In particular, this effect in LaMO<sub>3</sub> (M = Cr, Mn, Fe) has been shown to give rise to spin splitting<sup>63</sup>. LaMO<sub>3</sub> (M = Cr, Mn, Fe) is only one member of the perovskite structure where lattice distortion is commonly seen, therefore perovskites should be a zoo for altermagnetism, as reviewed by Naka *et al.*<sup>64</sup>.

After the work by Noda *et al.*<sup>60</sup>, theoretical studies of momentum-dependent spin splitting protected by crystal symmetry in collinear AFM have significantly advanced. Notable contributions include Naka *et al.* on 2D organic  $\kappa$ -Cl<sup>65</sup>, Ahn *et al.*<sup>66</sup> and Smekal *et al.*<sup>67</sup> on RuO<sub>2</sub>, Yuan *et al.*<sup>2</sup> and Egorov *et al.*<sup>68</sup> on MnF<sub>2</sub>, Ma *et al.*<sup>69</sup> on V<sub>2</sub>Se<sub>2</sub>O and Mazin *et al.*<sup>3</sup> on doped FeSb<sub>2</sub>, among others. Beyond SML, Šmekal *et al.*<sup>67</sup> demonstrated that collinear AFMs can exhibit AHE, a phenomenon traditionally associated only with ferromagnets. This property is particularly important for spintronics, as it enables the detection of magnetic states through electrical transport properties. Simultaneously, works by Naka *et al.*<sup>65</sup>, Shao *et al.*<sup>70</sup>, Rafael *et al.*<sup>71</sup>, Šmekal *et al.*<sup>72</sup> reported that spin currents along with SML can be generated in collinear AFMs, further highlighting their potentials in spintronics applications. As mentioned earlier, these fascinating phenomena has also been systematically explored within the framework of SAMB<sup>1,14,54</sup>.

Remarkably, the microscopic origin of staggered  $V_\sigma$  in the AFM phase has been explored using a *microscopic* Hubbard model by Naka *et al.*<sup>65</sup>. In  $\kappa$ -Cl the fundamental building units are two BEDT-TTF dimers, which are connected to each other via glide mirror symmetry. Since each BEDT-TTF molecule contributes one frontier orbital, a four-band (or eight-band including spin degree of freedom) Hubbard model can be constructed<sup>65</sup>:

$$\begin{aligned} \hat{H} = & U \sum_{i\mu} \hat{n}_{i\mu\uparrow} \hat{n}_{i\mu\downarrow} + t_a \sum_{i\sigma} (\hat{c}_{ia\sigma}^\dagger \hat{c}_{ib\sigma} + h.c.) \\ & + \sum_{\langle i,j \rangle \mu\mu'\sigma} t_{ij}^{\mu\mu'} (\hat{c}_{i\mu\sigma}^\dagger \hat{c}_{j\mu'\sigma} + h.c.) \end{aligned} \quad (16)$$

where  $i = 1, 2$  is the index for the two dimer inside a unit cell and  $\mu = a, b$  is the index for the two frontier orbital of a dimer. Within the Hartree approximation, increasing the on-site repulsion  $U$  drives a transition from a paramagnetic metal to an AFM metal. Across this phase transition, the glide-mirror-symmetric hopping present in the paramagnetic metal phase becomes broken in either the spin-up or spin-down channel of the AFM phase, but preserved in intra-spin channels. This resulting spin-dependent hoppings leads to SML.

## 3, Emergence of altermagnetism

As more exotic physical properties discovered in such type of collinear AFM (see recent reviews<sup>5–11</sup>), in 2022, Šmekal *et al.* proposed the idea of type-III collinear magnets, to be distinguished from the well-established known FM and collinear AFM. Type-III collinear magnets specify collinear magnets which have compensating magnetic moments in real space and momentum-dependent SML protected by crystal symmetry in the reciprocal space without SOC. Type-III collinear magnet was also termed altermagnetism<sup>4</sup>. Here, the prefix "alter" carries two distinct meanings. First, it refers to alternating orders in

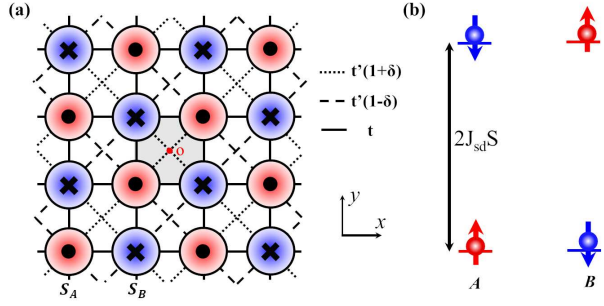


FIG. 5. (a) A Néel state on an alternating anisotropic square lattice is a  $d$ -wave altermagnet. It is invariant under  $[C_{2\perp}^{(s)}||C_{4z}^+]$  symmetry, where the red dot labels the rotation center. The shaded region is the paramagnetic unit cell. (b) Orbital interaction diagram for the two sublattices.

both real and reciprocal space: in real space, this reflects the compensating collinear magnetic moments; in reciprocal space, it signifies the alternating spin-splitting protected by crystal symmetry. In addition to this, "alter" also conveys the idea of alternating physical properties shared by FM and collinear AFM. Specifically, an "altermagnet" can exhibit characteristics typical of FM in one contexts, while simultaneously displaying behaviours associated with AFM in the others, as summarized by Mazin *et al.*<sup>73</sup>.

Following this thought, Liu *et al.*<sup>74</sup> proposed a second definition of unconventional magnetism: magnets adopt antiferromagnetic configurations yet display properties reminiscent of FMs. Within this framework, altermagnets (AMs) are considered a specific subset of unconventional magnets. Cheong *et al.*<sup>75,76</sup> defines altermagnetism more broadly as magnetism characterized by broken  $\mathcal{PT}$  symmetry, with a ground state exhibiting full spin compensation in the non-relativistic limit. This definition also includes noncollinear antiferromagnets and aligns with the conception of unconventional magnetism by Liu *et al.*<sup>74</sup>.

To grasp the key characteristics of AMs, we begin with a simple example of 2D square lattices shown in Fig.5(a) with two sublattices, which serves to introduce two ground-breaking insights — one by Hayami *et al.*<sup>1,14</sup> using the SAMB framework, and the other by Šmekal *et al.*<sup>4,5</sup> based on spin-group theory. Both perspectives are essential for developing a comprehensive understanding of AMs.

In Fig.5(a), we take the standard  $s-d$  model to incorporate the static AFM orders, which could be generated from on-site Hubbard repulsions as already explored by Das *et al.*<sup>77</sup>. The model Hamiltonian can then be rewrit-

ten as:

$$\begin{aligned}\hat{H}_{sd} = & -t \sum_{\langle i,j \rangle \sigma} (\hat{c}_{i\sigma}^\dagger \hat{c}_{j\sigma} + h.c.) - \sum_{\langle\langle i,j \rangle\rangle \sigma} t_{ij} (\hat{c}_{i\sigma}^\dagger \hat{c}_{j\sigma} + h.c.) \\ & - J_{sd} \sum_{i=A,B} \sum_{\sigma,\sigma'} \mathbf{S}_i \hat{c}_{i\sigma}^\dagger \boldsymbol{\sigma}_{\sigma\sigma'} \hat{c}_{i\sigma'} - \mu \sum_{i\sigma} \hat{c}_{i\sigma}^\dagger \hat{c}_{i\sigma}\end{aligned}\quad (17)$$

The nearest hopping  $t$  is isotropic while the next-nearest hoppings  $t_{ij}$  are anisotropic. As explicitly illustrated in Fig.5(a), they take values  $t'(1+\delta)$  or  $t'(1-\delta)$  along the  $(1,1)$ -direction or  $(1,-1)$ -direction for sublattice  $A$  with a dimensionless anisotropic parameter  $\delta < 1$ . For sublattice  $B$ , instead  $t_{ij} = t'(1-\delta)$  along the  $(1,1)$ -direction and  $t_{ij} = t'(1+\delta)$  along the  $(1,-1)$ -direction. In real materials, these anisotropic hoppings are actually "effective", and are obtained by integrating out the contributions of nonmagnetic ligand sites. In the last term of the model Hamiltonian, since we consider collinear AFM order, without loss of generality  $\mathbf{S}_i$  can be chosen to align along the  $z$  direction with magnitude  $+S$  and  $-S$  for sublattice  $A$  and  $B$ , respective. The coupling  $J_{sd}$  quantifies the on-site exchange interaction between the spin of the itinerant electrons and the localized spins on the magnetic sites  $\mathbf{S}_i$ .

After Fourier transformation, it is straightforward to see that the Hamiltonian becomes diagonal in spin space with the basis  $\Psi = (\hat{c}_{\mathbf{k}A\uparrow}, \hat{c}_{\mathbf{k}B\uparrow}, \hat{c}_{\mathbf{k}A\downarrow}, \hat{c}_{\mathbf{k}B\downarrow})^T$ :

$$\hat{H}_{sd} = \sum_{\mathbf{k}} \Psi^\dagger \hat{h}(\mathbf{k}) \Psi \quad (18)$$

with

$$\begin{aligned}\hat{h}(\mathbf{k}) = & -2t(\cos(k_x) + \cos(k_y))\sigma_0\tau_x - 4t'\cos(k_x)\cos(k_y) \\ & - 4t'\delta\sin(k_x)\sin(k_y)\sigma_0\tau_z - J_{sd}S\sigma_z\tau_z - \mu\end{aligned}\quad (19)$$

where the lattice constants are set to unity. The Pauli matrices  $\sigma_{x/y/z}$  and  $\tau_{x/y/z}$  describe the spin and sublattice degrees of freedom, respectively. The last two terms in  $\hat{h}(\mathbf{k})$  result from the anisotropic hoppings and collinear AFMs, respectively. Working together, these two terms lead to the spin-split band structure and SML. To see this, let us go through the key observations made by Hayami *et al.*<sup>1,14</sup>.

Hayami *et al.* first realized that the existence of  $[C_{2\perp}^{(s)}||\mathcal{T}]$  as we discussed earlier inspires a multipole expansion of the dispersion relation in terms of some conjugate fields, similar to  $X_{lm}^{ext}$  in Eq.12. The most crucial observation by Hayami *et al.* is that the collinear AFM ordering with sublattice degrees of freedom can activate particular conjugate fields, and hence can cause symmetry-breaking for the related multipoles. In other words, the collinear AFM ordering plays the role of a primary order parameter, and it induces multipole secondary order parameters, depending on the detailed crystal structure. This idea has been recently highlighted and

further developed by McClarty *et al.* to formulate a Landau theory for AMs<sup>78</sup>.

To better understand such a symmetry-breaking concept, it is useful to analyze the symmetry the 2D square lattice in Fig.5(a). At the paramagnetic phase, Fig.5(a) has point group  $C_{4v} = \{E, C_{4z}^+, \mathcal{P} = C_{2z}, C_{4z}^-, M_x, M_y, M_{11}, M_{1\bar{1}}\}$ , where  $C_{4z}^+/C_{4z}^-$  is the four-fold counterclockwise/clockwise rotation along the  $z$ -axis, and  $M_x/M_y/M_{11}/M_{1\bar{1}}$  denotes the mirror reflection perpendicular to  $x/y/(1,1)/(1,-1)$  direction. Since the horizontal mirror plane is redundant, the two-fold rotation along the  $z$ -axis  $C_{2z}$  is identical to the spatial inversion  $\mathcal{P}$ . At the collinear AFM phase, the Néel order transforms nontrivially under  $C_{4v}$ . It follows the 1D IR  $B_1$ , which takes the value "+1" under the invariant subgroup  $C_{2v} = \{E, C_{2z}, M_x, M_y\}$  and "-1" under the remaining element in coset  $C_{4z}^+ C_{2v}$ . As the same IRs are coupled with each other, the Néel order then induces a conjugate field associate with the multipole operator that transforms following  $B_1$ . This conjugate field leads to the spin-splitting in the band structure and hence SML. For a more detailed and rigorous treatment, see section V of Ref.<sup>14</sup>.

To explicitly examine the above statement, let us take the limit when the exchange strength  $J_{sd}$  is sufficiently large. When  $J_{sd}S$  is the largest energy scale of the model, we can safely keep  $\hat{c}_{\mathbf{kA}\uparrow}$ ,  $\hat{c}_{\mathbf{kB}\downarrow}$ , and ignore  $\hat{c}_{\mathbf{kA}\downarrow}$ ,  $\hat{c}_{\mathbf{kB}\uparrow}$  as they have a higher energy as shown in Fig.5(b). In the new basis  $\Psi = (\hat{c}_{\mathbf{kA}\uparrow}, \hat{c}_{\mathbf{kB}\downarrow})^T$ , the effective Hamiltonian is:

$$\begin{aligned} \varepsilon_\sigma(\mathbf{k}) = & -4t' \cos(k_x) \cos(k_y) - \mu - J_{sd}S \\ & - 4t' \delta \sin(k_x) \sin(k_y) \sigma_z \end{aligned} \quad (20)$$

You can find that the hoppings which are spin-independent but orientation-dependent in Eq.19 now acquire a spin dependent in Eq.20, which leads to spin splitting and SML. To explicitly contrast Eq.20 to the known expressions of multipole basis discussed earlier. To see this, we use  $\cos k \approx 1 - k^2/2$  and  $\sin k \approx k$  to expand the spectrum Eq.20 around  $\Gamma$  point:

$$\varepsilon_\sigma(\mathbf{k}) = E_0 + 2t' \mathbf{k}^2 - 4t' \delta k_x k_y \sigma \quad (21)$$

with the constant  $E_0 = -4t' - \mu - J_{sd}S$ . Eq.21 clearly shows the symmetry-breaking conjugate field associated with the **MT** quadrupole  $T_{xy}^{ext} = 2t' \delta$  (after transforming the paramagnetic unit cell to the magnetic supercell), in addition to the trivial conjugate field associated with the **E** monopole  $Q_0^{ext} = 2t'$ .

From above analysis, it is not difficult to construct general minimal models for AM, in the cases that a space group  $\mathbf{G}$  of the crystalline contains a halving group  $\mathbf{H}$  with  $\mathcal{P} \in \mathbf{H}$  and/or  $\tau \in \mathbf{H}$  and  $\mathbf{G} = \mathbf{H} \cup (\mathbf{G} - \mathbf{H}) = \mathbf{H} \cup A\mathbf{H}$  (where  $A \in \mathbf{G}$  is chosen that  $A\mathbf{H} \equiv \mathbf{G} - \mathbf{H}$ ). By considering a 1D IR of the site symmetry group for sublattice degrees of freedom, Roig *et al.* developed forty such models for 3D AMs in the form<sup>79</sup>:

$$\hat{h}(\mathbf{k}) = \varepsilon_0(\mathbf{k}) + t_x(\mathbf{k}) \tau_x + t_z(\mathbf{k}) \tau_z + \mathbf{J} \cdot \boldsymbol{\sigma} \tau_z + \boldsymbol{\lambda}(\mathbf{k}) \cdot \boldsymbol{\sigma} \tau_y \quad (22)$$

with a sublattice independent dispersion  $\varepsilon_0(\mathbf{k})$ , inter- and intrasublattice hopping coefficients  $t_x(\mathbf{k})$  and  $t_z(\mathbf{k})$ , a primary order parameter  $\mathbf{J}$ , and a SOC term  $\boldsymbol{\lambda}(\mathbf{k})$ . The form of  $\boldsymbol{\lambda}(\mathbf{k})$  can be determined by considering the transformation properties of the sublattice operator  $\tau_y$  (which follows the same 1D IR at  $\tau_z$ ) and of the spin operator  $\boldsymbol{\sigma}$ , under the space group  $\mathbf{G}$ .

Finally, let us briefly mention the spin-group analysis by Šmejkal *et al.*<sup>4</sup>, which was already well-documented by several reviews<sup>6,10</sup>. The key observation by Šmejkal *et al.*<sup>4</sup> is the existence of the following symmetry operations,

$$[E||\mathbf{H}] + [C_{2\perp}^{(s)}||A\mathbf{H}] \quad (23)$$

in the spin group the lattice structure. In the 2D square lattice shown in Fig.5(a), we have  $\mathbf{G} = C_{4v}$ ,  $\mathbf{H} = C_{2v}$ , and  $A = C_{4z}^+$ . These symmetries are crucial in determining the characteristic anisotropy of the spin density distribution on each sublattice. For example, the symmetry operations  $[C_{2\perp}^{(s)}||A\mathbf{H}]$  guarantees the exchange between sublattices with opposite spin orientations, thereby enforcing a vanishing net magnetization - similar to conventional AFM. However, the coset  $A\mathbf{H}$  does not contain  $\mathcal{P}$  (which is already one element of  $\mathbf{H}$ ), indicating the broken of  $\mathcal{T}$ . For a generic wave-vector  $\mathbf{k}$ , its little group also lacks the element of  $A\mathbf{H}$ , implying the spin-split band structure, reminiscent of FM. The symmetry operation in Eq.23 thereby define the magnetic order of AM, different from either AFM or FM. They also provide a useful alternative description of the collinear AFM ordering induced symmetry breaking, from a symmetry point of view based on the powerful tool of spin-group theory<sup>80-86</sup>.

In this context, it is worth highlighting several recent developments of spin-group theory as applied to AMs and the related phenomena. In 2022, Liu *et al.*<sup>15</sup> classified spin point groups for collinear, coplanar, and non-coplanar configurations. More recently, in 2024, three independent groups systematically enumerated the spin space groups and their representation<sup>87-89</sup>. It is also noteworthy that the concept of spin groups has been widely employed in describing quantum phase transition in spin systems, particularly in the limit where SOC vanishes. For instance, in the quantum Heisenberg model  $\hat{H} = \sum_{\langle i,j \rangle} J_{ij} \hat{\mathbf{S}}_i \cdot \hat{\mathbf{S}}_j$  for an example, the Hamiltonian remains invariant under a global rotation of all spins by an arbitrary angle.

#### 4, Relationship to the previous subsections

We now turn to connecting AMs with the ELC phases and multipole expansions discussed in the previous subsections. For AM metals, they have spin-momentum locked FSs resemble those found in  $F_{l>1}^A$  channel  $\alpha$  phase (see Fig.2) or characterized by distinct multipoles (see Fig.3). Accordingly, the type of SML is labeled by the angular momentum quantum number  $l$  and for

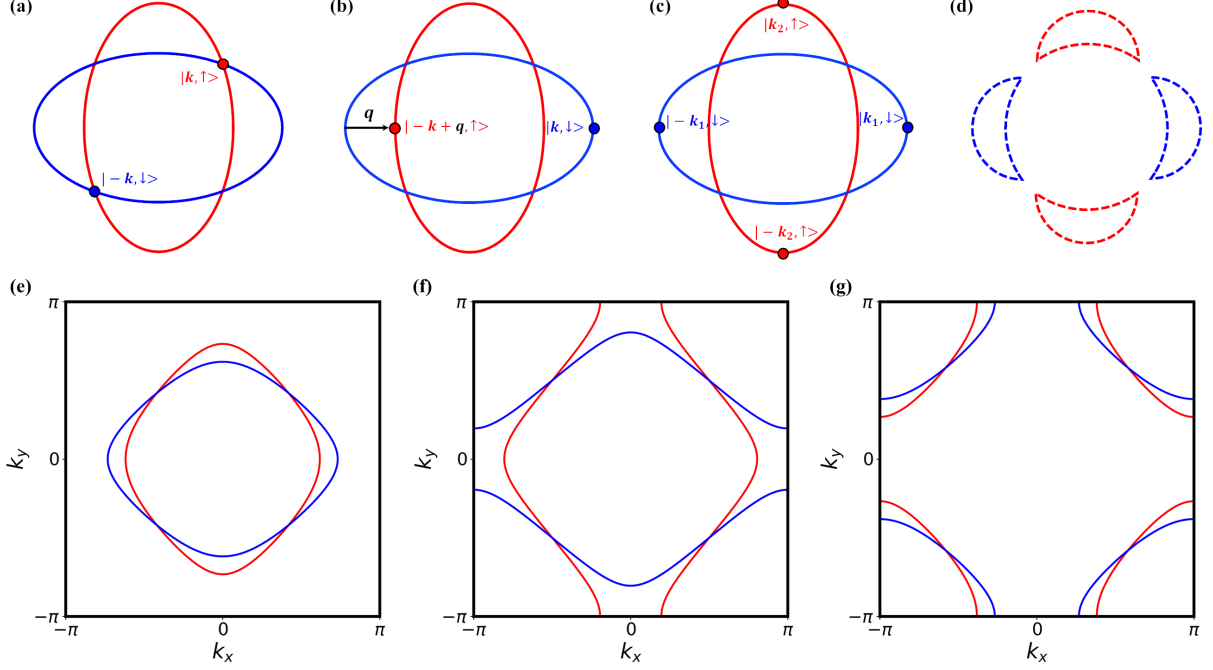


FIG. 6. Demonstration of different pairing possibilities of  $d_{x^2-y^2}$ -wave SML in either continuum model or 2D square lattice. (a) Spin-singlet  $s$ -wave paring. (b) Finite center-of-mass momentum pairing. (c) Spin-triplet  $p$ -wave paring. (d) Schematic representation of Bogoliubov Fermi surface, where the dashed lines indicate regions with zero-energy Bogoliubov quasiparticle excitations. (e)-(g) Fermi surfaces of 2D square lattice at low, half, and high fillings, respectively

$l = 0, 1, 2, 3, \dots$ , we have  $s$ -,  $p$ -,  $d$ -,  $g$ -wave SML<sup>4</sup>. However, it is important to note that these  $F_l^A$  channel spin-momentum locked FSs - or more generally, multiple expansions - are constructed with a single-band framework, which does not apply to AMs. In AMs, the requirement of compensated magnetic moments implies the presence of at least two sublattices (with the exact number determined by the underlying spin space group). Consequently, a multiband description is necessary to capture the Fermi surface topology. For the same reason, atomic multipole descriptions are insufficient; instead, SAMB is required to fully describe AMs, as seen in the works by Hayami *et al.*<sup>1,14</sup>.

We finally note that, the origin of spin-momentum locked FSs from PI instability remains poorly understood. Theoretically, determining Landau parameters in strongly correlated electronic systems is notoriously challenging, especially when a sublattice degree of freedom is involved. Investigating the potential for PI-induced AMs in future studies would be highly intriguing.

### III. SUPERCONDUCTIVITY WITH SPIN-MOMENTUM LOCKED FERMI SURFACES

As mentioned in previous section, the name ELC phase is inspired by the experimental observation of smectic phases in high- $T_c$  superconductors. Although the spin nematic phase has not been found at that time, theoret-

ical predictions about the SC in spin nematic phase has been explored, as we show below.

Before going into detailed discussions, by simple inspection at the spin-momentum locked FSs shown in Fig.6(a), we can anticipate three different Cooper pairings. The first one comes from zero-momentum spin-singlet pairing due to states  $|k, \uparrow\rangle$  and  $|-k, \downarrow\rangle$ , as marked in Fig.6(a). This is expected to happen at strong pairing and weak anisotropic spin splitting regime and gives either  $s$ -wave or  $d$ -wave SC. The second one is the finite-momentum pairing, where the two mismatched FSs is connected by a finite momentum  $\mathbf{q}$  as shown Fig.6(b). Such a state is an unpolarized analog of the FFLO state<sup>90,91</sup>, here we still call it FFLO state (this state is also a type of pair-density-wave states). The third one is the zero-momentum spin-triplet pairing attributing to states  $|k_1, \uparrow\rangle$  and  $|-k_1, \uparrow\rangle$  ( $|k_2, \uparrow\rangle$  and  $|-k_2, \uparrow\rangle$ ) as shown Fig.6(c). Such spin-triplet pairing is unitary due to zero net magnetization<sup>92</sup>. The above simple inspection suggests that SC in AMs can resemble that in either FM or AFM systems.

Fig.7 summarizes the landscape related to SC with SML, which includes superconducting diode effect<sup>93-97</sup>, Josephson effect<sup>98-103</sup>, Andreev reflection<sup>104-107</sup>, Majorana zero mode<sup>108-112</sup>, Floquet superconductivity<sup>113-115</sup> and many others. We note that, recently, Fukaya *et al.*<sup>116</sup> have reviewed the latest developments on superconducting phenomena in systems with unconventional magnets, especially on transport properties based on su-

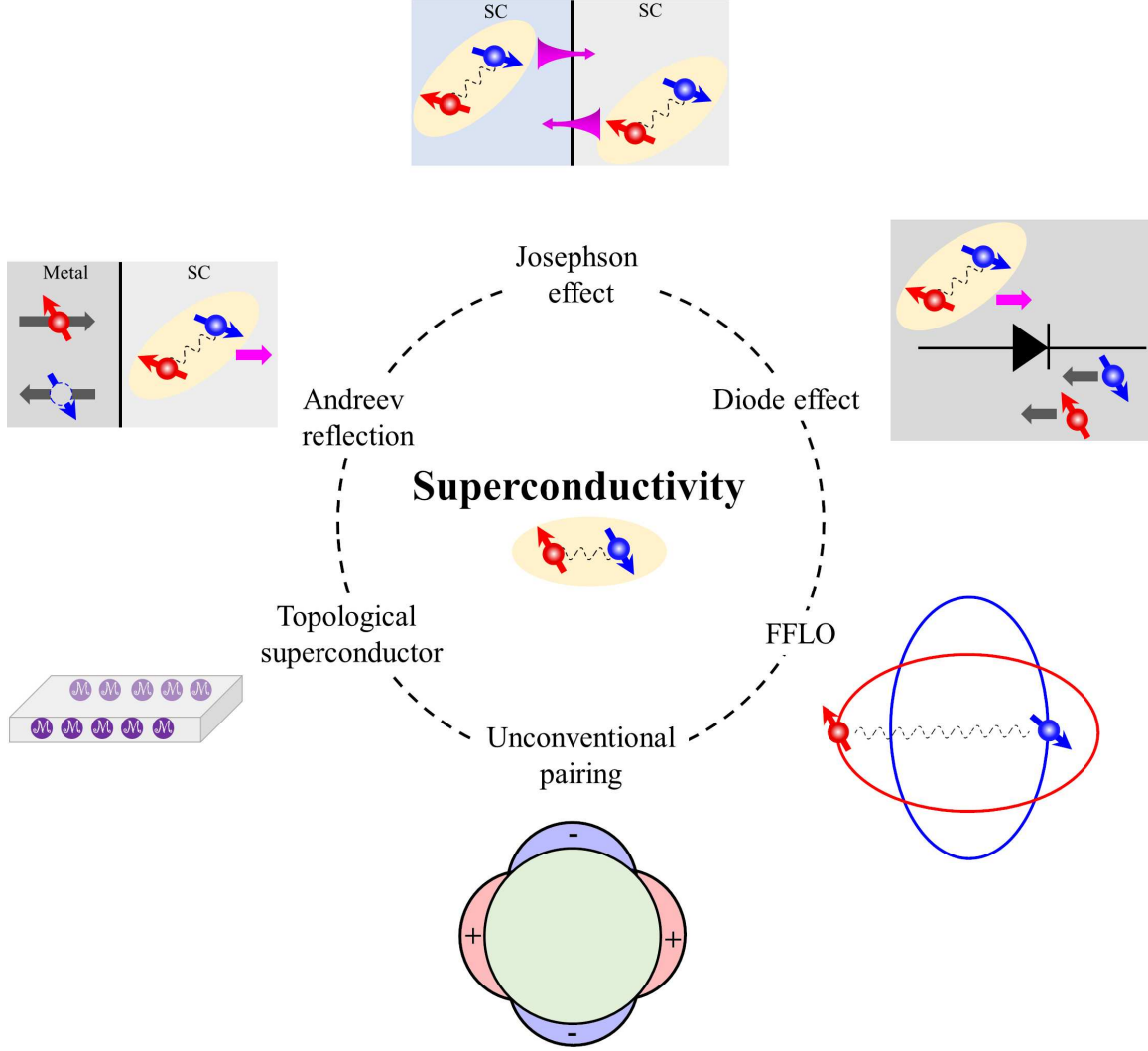


FIG. 7. Emerging research landscape of superconductivity related to altermagnetism.

perconducting junctions.

In the following, we focus on two key topics: (1) spin-singlet finite-momentum pairing mediated by attractive interaction with  $s$ - and  $d$ -wave symmetry, and (2) spin-triplet superconductivity, which is closely associated with topological superconducting phases. Our analysis is based on a one-band model, which, despite being an approximation in AMs, captures the essential features of SML and serves as a minimal framework for exploring the resulting exotic pairing phenomena. In AMs,  $s$ -wave pairing may arise either from the intrinsic electron-phonon coupling or via the proximity effect through coupling with conventional superconductors.

To describe the superconducting order parameter, we employ the standard Bogoliubov-de Gennes (BdG) mean-field approximation. This approach is reliable when fermions interactions are not excessively strong. Accordingly, throughout our discussion of the two topics, we assume that the attractive interactions are of weak to

medium strength relative to the Fermi energy.

#### A. FFLO states with attractive pairing

##### 1, $s$ -wave pairing potential

In 2009, Feiguin *et al.*<sup>117</sup> considered the spin-dependent hopping in 2D square lattices subject to  $s$ -wave pairing instability, as described by the model Hamiltonian:

$$H = \sum_{\mathbf{k},\sigma} \varepsilon_{\sigma}(\mathbf{k}) \hat{c}_{\mathbf{k}\sigma}^{\dagger} \hat{c}_{\mathbf{k}\sigma} + U \sum_i \hat{n}_{i\uparrow} \hat{n}_{i\downarrow}, \quad (24)$$

where

$$\varepsilon_{\uparrow}(\mathbf{k}) = -2t_a \cos(k_x) - 2t_b \cos(k_y) - \mu, \quad (25a)$$

$$\varepsilon_{\downarrow}(\mathbf{k}) = -2t_b \cos(k_x) - 2t_a \cos(k_y) - \mu, \quad (25b)$$

where  $t_a$  and  $t_b$  are two hopping strengths determining the anisotropy of the two elliptical FSs (see below),  $U < 0$  is the onsite attractive interaction. Such a Hamiltonian exhibits  $C_{4z}\mathcal{T}$  symmetry with anisotropic spin splitting controlled by  $t_b/t_a$  (without the loss of generality,  $t_b/t_a < 1$  is taken). At small lattice filling factors, the two Fermi ellipses are centered at  $\Gamma$  point as shown in Fig.6(e). Expanding around  $\Gamma$  point,  $\cos(k_x) \approx 1 - \frac{1}{2}k_x^2$ ,  $\cos(k_y) \approx 1 - \frac{1}{2}k_y^2$ , and defining

$$Q_0^{ext} \equiv \frac{t_a + t_b}{2}, T_{xy}^{ext} \equiv \frac{t_a - t_b}{2} \quad (26)$$

the single-particle energy Eq.25a and Eq.25b can be expressed uniformly as

$$\varepsilon_\sigma(\mathbf{k}) = Q_0^{ext}\mathbf{k}^2 + \sigma T_{xy}^{ext}(k_x^2 - k_y^2) - 2(t_a + t_b) - \mu \quad (27)$$

which has **E** monopole and **MT** quadrupole as defined in the previous section. Isotropic hopping occurs when  $t_a = t_b$ , thus  $T_{xy}^{ext}$  measures the anisotropic spin splitting.

At half-filling, the FSs become opened, as shown in Fig.6(f). This filling level is particularly noteworthy due to the presence of a van Hove singularity - a logarithmic divergence in the density of states - in the paramagnetic phase. As the filling increases beyond half-filling, the open FSs evolve into closed ones center at  $M$  point as shown in Fig.6(g). By fixing the interaction strength of  $|U|$  and applying the self-consistent BdG mean-field approximation, Feiguin *et al.* mapped out the ground state phase diagram with respect to  $t_b/t_a$  and electron filling (up to half filling). For a dimensionless pairing interaction of  $U/t_a = -3.5$ , four distinct phases emerge: a conventional Bardeen-Cooper-Schrieffer (BCS) superfluid (SF); a phase-separated region at medium  $t_b/t_a$  and filling, a nodal SF at small  $t_b/t_a$  and intermediate filling, and a normal (nonsuperconducting) phase at small  $t_b/t_a$  and high filling. The nodal SF arises due to vanishing Bogoliubov quasiparticle excitation energy at specific momenta, as indicated in Fig.6(d). These gapless excitations form what is referred to as Bogoliubov Fermi surface (BFS)<sup>118</sup>, due to their resemblance to conventional

FSs. When the pairing interaction is increased further to  $U/t_a = -4$ , both phase-separated and normal phase vanish where BCS SF becomes the ground state. Such a fact matches the fact that strong attractive interaction favours conventional SC. Notably, the FFLO states, which is of particular interest, does not appear within the range of parameters explored in this study.

In 2014, Soto-Garrido *et al.*<sup>119</sup> studied the possible FFLO states in a similar but continuum model to that of Feiguin *et al.*<sup>117</sup>. The single-particle Hamiltonian is:

$$\mathcal{H} = \sum_{\mathbf{k}\alpha\beta} \hat{c}_{\mathbf{k}\alpha}^\dagger [\varepsilon_{\mathbf{k}} + T_{xy}^{ext}(k_x^2 - k_y^2)(\sigma_z)_{\alpha\beta}] \hat{c}_{\mathbf{k}\beta} \quad (28)$$

with the following interaction:

$$\mathcal{H}_{int} = -U \sum_{\mathbf{k}, \mathbf{k}', \mathbf{q}} \hat{c}_{\mathbf{k}+\mathbf{q}/2\uparrow}^\dagger \hat{c}_{-\mathbf{k}+\mathbf{q}/2\downarrow}^\dagger \hat{c}_{-\mathbf{k}'+\mathbf{q}/2\downarrow} \hat{c}_{\mathbf{k}'+\mathbf{q}/2\uparrow} \quad (29)$$

Here,  $T_{xy}^{ext} < 1$  is now a dimensionless parameter. The Fourier transformation of the pairing interaction in Eq.24 takes the same form as Eq.29, therefore Eq.28 and Eq.29 can be understood as the dilute limit of the 2D square lattice model.

At temperature  $T$ , the superconductivity susceptibility  $\chi_{sc}(\mathbf{Q}, i\nu_n)$  can be calculated by summing all the bubble diagrams in the particle-particle channel:

$$\begin{aligned} \chi_{sc}(\mathbf{Q}, i\nu_n) = k_B T \sum_{n=-\infty}^{\infty} \int \frac{d\mathbf{k}}{(2\pi)^2} G_0(\mathbf{k} + \frac{\mathbf{Q}}{2}, i\omega_m + i\nu_n/2) \\ \times G_0(-\mathbf{k} + \frac{\mathbf{Q}}{2}, -i\omega_m + i\nu_n/2) \end{aligned} \quad (30)$$

where  $k_B$  is the Boltzmann constant,  $\mathbf{Q}$  is the center-of-mass momentum of Cooper pairs,  $\omega_m = (2m+1)\pi k_B T$  are fermionic Matsubara frequencies,  $\nu_n = 2n\pi k_B T$  are bosonic Matsubara frequencies, and

$$G_0(\mathbf{k}, i\omega_m) = \frac{1}{i\omega_m - \varepsilon(\mathbf{k})} \quad (31)$$

is the free-fermion Green's function. After performing the Matsubara sum in Eq.30 we yield

$$\chi_{sc}(\mathbf{Q}, i\nu_n) = \int \frac{d\mathbf{k}}{(2\pi)^2} \frac{1 - n_F(\varepsilon(\mathbf{k} + \mathbf{Q}/2)) - n_F(\varepsilon(-\mathbf{k} + \mathbf{Q}/2))}{\varepsilon(\mathbf{k} + \mathbf{Q}/2) + \varepsilon(-\mathbf{k} + \mathbf{Q}/2) - i\nu_n} \quad (32)$$

---

where  $n_F(\varepsilon) = \frac{1}{1+e^{\varepsilon/k_B T}}$  is the Fermi-Dirac distribution. At finite temperature, Eq.32 in general has to be evaluated numerically. However, at zero temperature it is possible to obtain explicit analytic expressions for the

---

pairing susceptibility at zero frequency, which gives us the well-known Thouless criterion for the onset of SC. Applying analytical continuation  $i\nu_n = \nu + i0^+$  and setting  $\nu = 0$ , we obtain the zero-temperature expression:

---

$$\chi_{sc}(\mathbf{Q}) = \int \frac{d\mathbf{k}}{(2\pi)^2} \frac{1 - \Theta(-\varepsilon(\mathbf{k} + \mathbf{Q}/2)) - \Theta(-\varepsilon(-\mathbf{k} + \mathbf{Q}/2))}{\varepsilon(\mathbf{k} + \mathbf{Q}/2) + \varepsilon(-\mathbf{k} + \mathbf{Q}/2)} \quad (33)$$

where  $\Theta(x)$  is the Heaviside step function.

To proceed, Soto-Garrido *et al.* assumes that the integration over  $\mathbf{k}$  can be approximated as:

$$\int \frac{d\mathbf{k}}{(2\pi)^2} \rightarrow N_F \int_{-\omega_D}^{\omega_D} d\zeta \int_0^{2\pi} \frac{d\theta}{2\pi} \quad (34)$$

where  $\omega_D$  is an energy cutoff. Such an approximation implies that only a finite region near the FS contributes to pairing susceptibility, in line with the spirit of BCS theory. Using Eq.34, Eq.33 can be integrated as:

$$\chi_{sc}(\mathbf{Q}) = N_F \int_0^{2\pi} \frac{d\theta}{2\pi} \ln \left| \frac{\omega_D}{T_{xy}^{ext} \cos(2\theta) - \frac{Q}{2} \cos(\theta - \phi)} \right| \quad (35)$$

where  $Q$  (in units of the Fermi wave-vector  $k_F$ ) and  $\phi$  are the magnitude and the polar angle of  $\mathbf{Q}$ . By choosing  $\phi = n\pi/2$ , i.e.  $\mathbf{Q}$  is along either  $x$ -axis or  $y$ -axis in Fig.6(a),  $\chi_{sc}(Q)$  is flat for  $Q \leq 2T_{xy}^{ext}$  and decreases for  $Q > 2T_{xy}^{ext}$ . Therefore, there is no preference for a finite value of  $Q$  in this situation, which exclude the possibility of a FFLO state. This result seems to be in accordance with that of Feiguin *et al.*<sup>117</sup> at low filling.

The recent discovery of  $d$ -wave AMs has revived interest in realizing FFLO states with spin-momentum locked FSs. In 2024, Chakraborty *et al.*<sup>120</sup> studied the 2D square lattice model with different  $s$ -wave pairing interaction strengths and different filling factors, and found the absence of FFLO state. At the same time, Zhang *et al.*<sup>121</sup> studied the 2D continuum model and obtained an analytical expression for the critical  $\mathbf{Q}$  ( $\mathbf{Q}_c$ ) at the large chemical potential limit. Using  $T_{xy}^{ext}$  as the altermagnetic spin splitting, the magnitude of  $\mathbf{Q}_c$  is expressed as:

$$Q_c(\phi) = \pm \left[ \sqrt{\frac{\mu}{1 + T(\phi)}} - \sqrt{\frac{\mu}{1 - T(\phi)}} \right] \quad (36)$$

where  $T(\phi) = T_{xy}^{ext} \cos(2\phi)$  and the chemical potential  $\mu$  is measured in units of the Fermi energy,  $\varepsilon_F$ . Eq.36 gives an anisotropic  $\phi$ -dependent  $\mathbf{Q}_c$ . With  $\phi = \pi/4 + n\pi/2$ ,  $Q_c = 0$ , therefore no FFLO states are preferred. However, when  $\mathbf{Q}$  is along  $x$ -axis or  $y$ -axis,  $\phi = n\pi/2$ ,  $Q_c$  reaches the maximum value  $|\sqrt{\mu/(1 + T_{xy}^{ext})} - \sqrt{\mu/(1 - T_{xy}^{ext})}|$ , indicating the existence of a FFLO state. In this case, the value of the threshold  $Q_c$  can be well-understood geometrically as the length of the arrow shown in Fig.6(b), as pointed out recently by Liu *et al.*<sup>122</sup>. This finding by Zhang *et al.*<sup>121</sup> obviously disagrees with the results by Feiguin *et al.*<sup>117</sup>, Soto-Garrido *et al.*<sup>119</sup>, and Chakraborty *et al.*<sup>120</sup>. In 2025, Hong *et al.*<sup>123</sup> studied the 2D square lattice model at a moderate interaction strength and at low filling factors, and found

a phase transition from a BCS state to the FFLO phase increasing  $T_{xy}^{ext}$ . Sim *et al.*<sup>95</sup> and Hu *et al.*<sup>124</sup> investigated the 2D continuum model numerically and confirmed the results of Hong *et al.*<sup>123</sup>.

To clarify the above controversial results, most recently, Liu *et al.*<sup>122</sup> carried out an analytical study of the 2D continuum model. Without any approximation, the ground state phase diagram has been obtained at both fixed chemical potential and fixed total particle number. In both cases, FFLO states do exist, in accordance with Zhang *et al.*<sup>121</sup>, Hong *et al.*<sup>123</sup>, and Hu *et al.*<sup>124</sup>. Liu *et al.*<sup>122</sup> clearly showed that the flatness of  $\chi_{sc}(Q)$  in Eq.35 is due to the approximation made in Eq.34. If the full  $\mathbf{k}$  integration is taken at all the energy scales without any approximation, then,  $\chi_{sc}(Q)$  should increases slowly as  $Q$  increases below the threshold  $Q_c$  given in Eq.36. Moreover, Liu *et al.*<sup>122</sup> can repeat the phase diagram of Hong *et al.*<sup>123</sup> and Hu *et al.*<sup>124</sup>. Finally, Liu *et al.*<sup>122</sup> demonstrated that a nodeless SF with topological BFS emerges when the chemical potential is fixed.

At present, we could give an affirmative conclusion that the FFLO phase can be induced by  $d$ -wave altermagnetic spin splitting in two-dimensional spin-1/2 Fermi systems with attractive  $s$ -wave pairing interactions.

## 2, $d$ -wave pairing potential

Having first considered the conventional  $s$ -wave pairing potential, we now turn our attention to the  $d$ -wave pairing potential. In 2D, both the  $d$ -wave SML and  $d$ -wave pairing potential can exhibit either  $d_{x^2-y^2}$  or  $d_{xy}$  symmetry. This lead to possible configurations, depending on the relative orientation between SML and pairing potential. In the following, we fix the pairing potential to have  $d_{x^2-y^2}$  symmetry. The two corresponding cases - with  $d_{x^2-y^2}$ -wave or  $d_{xy}$ -wave SML - are schematically illustrated in Fig.8. In Fig.8(a), the  $d_{x^2-y^2}$ -wave SML leads to pairing nodes that coincide with the intersection point between the two elliptic FSs. In contrast, Fig.8(b) shows that for the  $d_{xy}$ -wave SML, the strongest pairing occurs at the four interaction points of the two elliptic FSs.

The  $d$ -wave pairing potential can arise from the nearest attractive interaction<sup>125</sup>. Let us consider the extended attractive Hubbard model on 2D square lattice:

$$\mathcal{H}_{int} = -U \sum_i \hat{n}_{i\uparrow} \hat{n}_{i\downarrow} - V \sum_{\alpha\beta} \sum_{\langle i,j \rangle} \hat{n}_{i\alpha} \hat{n}_{j\beta} \quad (37)$$

By setting the distance of nearest neighbors to be unity, after Fourier transformation, we have

---


$$\mathcal{H}_{int} = -\frac{1}{N} \sum_{\mathbf{k}, \mathbf{k}', \mathbf{q}} \sum_{\alpha\beta} V_{\alpha\beta} (\mathbf{k} - \mathbf{k}') \hat{c}_{\mathbf{k} + \frac{\mathbf{q}}{2}\alpha}^\dagger \hat{c}_{-\mathbf{k} + \frac{\mathbf{q}}{2}\beta}^\dagger \hat{c}_{-\mathbf{k}' + \frac{\mathbf{q}}{2}\beta} \hat{c}_{\mathbf{k}' + \frac{\mathbf{q}}{2}\alpha} \quad (38)$$

where  $N$  is the total number of sites on the lattice and

$$V_{\alpha\beta}(\mathbf{k} - \mathbf{k}') = U(1 - \delta_{\alpha\beta}) + 2V[\cos(k_x - k'_x) + \cos(k_y - k'_y)] \quad (39)$$

Using the spherical harmonics decomposition on square lattices:

$$\begin{aligned} g_s(\mathbf{k}) &= 1 \\ g_{es}(\mathbf{k}) &= \cos(k_x) + \cos(k_y) \\ g_{p\pm ip}(\mathbf{k}) &= \sin(k_x) \pm i\sin(k_y) \\ g_d(\mathbf{k}) &= \cos(k_x) - \cos(k_y) \end{aligned} \quad (40)$$

here "es" means extended  $s$ -wave, and noticing that

$$2[\cos(k_x - k'_x) + \cos(k_y - k'_y)] = \sum_m g_m(\mathbf{k})g_m^*(\mathbf{k}') \quad (41)$$

where  $m$  labels different square harmonics ( $s$ ,  $es$ ,  $p \pm ip$ ,  $d$ ), the extended attractive interaction Hamiltonian can then be decomposed into different pairing channels:

$$\begin{aligned} \mathcal{H}_{int} &= -\frac{1}{N} \sum_{\mathbf{k}, \mathbf{k}', \mathbf{q}, m, \alpha, \beta} \lambda_{\alpha\beta}^m g_m(\mathbf{k})g_m^*(\mathbf{k}') \\ &\times \hat{c}_{\mathbf{k}+\frac{\mathbf{q}}{2}\alpha}^\dagger \hat{c}_{-\mathbf{k}+\frac{\mathbf{q}}{2}\beta}^\dagger \hat{c}_{-\mathbf{k}'+\frac{\mathbf{q}}{2}\beta} \hat{c}_{\mathbf{k}'+\frac{\mathbf{q}}{2}\alpha} \end{aligned} \quad (42)$$

with

$$\lambda_{\alpha\beta}^s = U(1 - \delta_{\alpha\beta}), \lambda_{\alpha\beta}^{es/p\pm ip/d} = V \quad (43)$$

When  $V = 0$ , we have only  $s$ -wave pairing, which has been discussed in previous section. When  $V \neq 0$ , other partial-wave pairings become possible. In particular, the

$d_{x^2-y^2}$ -wave pairing potential mentioned at the beginning of this subsection, i.e.,  $g_d(\mathbf{k})$ , appears in this square harmonics decomposition.

We can tailor Eq.43 to select a particular paring potential. For example, if we choose

$$\begin{aligned} \lambda_{\uparrow\downarrow}^{es/p\pm ip/d} &= \lambda_{\downarrow\uparrow}^{es/p\pm ip/d} = V \\ \lambda_{\uparrow\uparrow}^{es/p\pm ip/d} &= \lambda_{\downarrow\downarrow}^{es/p\pm ip/d} = 0 \end{aligned} \quad (44)$$

then the extended  $s$ -wave and  $d_{x^2-y^2}$ -wave pairing potentials are allowed while  $p \pm ip$ -wave pairing potentials are forbidden. These two attractive interaction potentials will couple opposite spins at nearest neighbors, resulting the spin-singlet SC. Alternatively, we can choose

$$\begin{aligned} \lambda_{\uparrow\downarrow}^{es/p\pm ip/d} &= \lambda_{\downarrow\uparrow}^{es/p\pm ip/d} = 0 \\ \lambda_{\uparrow\uparrow}^{es/p\pm ip/d} &= \lambda_{\downarrow\downarrow}^{es/p\pm ip/d} = V \end{aligned} \quad (45)$$

then the  $p \pm ip$ -wave pairing potentials are allowed while the extended  $s$ -wave and  $d_{x^2-y^2}$ -wave pairing potentials are forbidden. In the case that all the pairing potentials are present simultaneously, they compete with one another, and the resulting superconducting state is determined by the channel that becomes unstable first as the temperature decreases.

In 2014, Soto-Garrido *et al.*<sup>119</sup> also studied the  $d_{x^2-y^2}$ -wave pairing potential with  $d_{x^2-y^2}$ -wave SML with the continuum model, by setting  $\lambda_{\uparrow\downarrow}^d = \lambda_{\downarrow\uparrow}^d = V$  and suppressing all the other channels in Eq.42. As discussed in the above, such a choice corresponds to spin singlet  $d_{x^2-y^2}$ -wave pairing. In this case, the pairing susceptibility can be expressed as:

$$\chi_{sc}(\mathbf{Q}) = N_F \int_0^{2\pi} \frac{d\theta}{2\pi} \cos^2(2\theta) \ln \left| \frac{\omega_D}{T_{xy}^{ext} \cos(2\theta) - \frac{Q}{2} \cos(\theta - \phi)} \right| \quad (46)$$

By choosing  $\phi = n\pi/2$ ,  $\chi_{sc}(Q)$  increases for  $Q \leq 2T_{xy}^{ext}$  and then decreases for  $Q > 2T_{xy}^{ext}$ . Therefore, one obtains a threshold  $Q_c = 2T_{xy}^{ext}$  and the inhomogeneous FFLO state with centre-of-mass momentum  $Q_c$  becomes the ground state.

More recently, this result was explicitly examined by Chakraborty *et al.*<sup>120</sup>, by numerically investigating a 2D square lattice model and by setting  $\lambda_{\uparrow\downarrow}^{es/d} = \lambda_{\downarrow\uparrow}^{es/d} = V/2$

only in Eq.42. They found that when  $V/Q_0^{ext} \approx 2$  and the filling is around 0.6, the FFLO state emerges as the ground state within a narrow range of  $T_{xy}^{ext}$ , provided that the modulation vector  $\mathbf{Q}$  is aligned along either  $x$ -axis or  $y$ -axis.

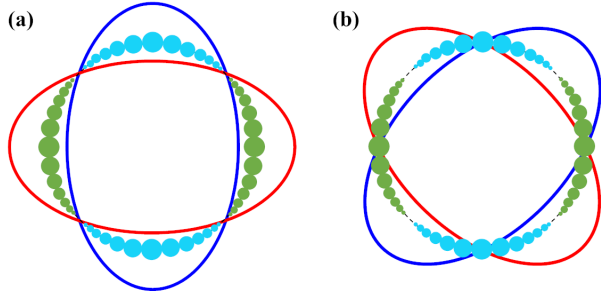


FIG. 8. Two possible orientation of  $d$ -wave SC and  $d$ -wave SML: (a) both SC and SML are  $d_{x^2-y^2}$ -wave; (b) SC is  $d_{x^2-y^2}$ -wave while SML is  $d_{xy}$ -wave. The colored lines and solid circles represent SML and SC components, respectively.

### B. Spin-triplet superconductivity

Let us finally turn to the spin-triplet SC with  $d$ -wave SML. In 2014, Gukelberger *et al.*<sup>126</sup> revisited the lattice model originally proposed by Feiguin *et al.*<sup>117</sup>. Using diagrammatic Monte Carlo simulations to perform an unbiased sampling of the Feynman diagrammatic series, they uncovered a rich phase diagram. At the filling factors of 1.2 (equivalent to 0.8 due to particle-hole symmetry) and at low temperatures, four distinct phases were identified: a BCS SF, two different  $p$ -wave triplet SFs, and an incommensurate density wave. Notably, in the absence of a nearest attractive interaction, the two  $p$ -wave spin-triplet SFs emerge only as second-order perturbative effect. These phases are stabilized only at sufficiently low temperatures, where competing instabilities are suppressed.

In 2023, Zhu *et al.*<sup>127</sup> considered the possibility of  $p$ -wave superconductivity in 2D altermagnetic metals. It is well known that Rashba SOC can turn a  $s$ -wave SC into  $p$ -wave. Therefore, the following single-particle Hamiltonian with Rashba SOC is considered,

$$\begin{aligned} \mathcal{H}_0 &= \sum_{\mathbf{k}\alpha\beta} h_{\alpha\beta}(\mathbf{k}) \hat{c}_{\alpha}^{\dagger}(\mathbf{k}) \hat{c}_{\beta}(\mathbf{k}) \\ h(\mathbf{k}) &= -2Q_0^{ext} g_{es}(\mathbf{k}) \sigma_0 - 2T_{xy}^{ext} g_d(\mathbf{k}) \sigma_z \\ &\quad + 2Q_z^{ext} (\text{sink}_y \sigma_x - \text{sink}_x \sigma_y) \end{aligned} \quad (47)$$

where  $Q_z^{ext}$  being the strength of Rashba SOC. For the interaction part, Zhu *et al.*<sup>127</sup> adopted the following form:  $\lambda_{\alpha\beta}^s = U(1 - \delta_{\alpha\beta})$ ,  $\lambda_{\uparrow\uparrow}^{s/es/p\pm ip/d} = \lambda_{\downarrow\downarrow}^{s/es/p\pm ip/d} = V$ . In the absence of Rashba SOC, and under conditions of weak SML and low filling, increasing the interaction  $V$  drives a transition from  $s$ -wave to  $p$ -wave superconductivity. When Rashba SOC is included,  $\mathcal{P}$  is broken, leading to a mixing of  $s$ -wave and  $p$ -wave components in the superconducting order parameter.

In 2025, Hong *et al.*<sup>123</sup> extended the analysis by considering the full set of interaction potentials in Eq.37, rather than limiting the model to spin-singlet or spin-triplet pairing alone. By fixing an intermediate on-site attractive interaction  $U$  and working at filling, they found that

$p + ip$ -wave superconductivity typically occurs when the nearest-neighbor interaction  $V$  exceeds a critical threshold  $V_c$ . This threshold  $V_c$  initially decreases rapidly with increasing  $T_{xy}^{ext}$ , and then saturates at large values of  $T_{xy}^{ext}$ .

## IV. DISCUSSION AND OUTLOOK

Thus far, we have highlighted the two themes: (1) the heuristic development of novel magnetic order of AM, and (2) the ensuing exotic superconductivity. In this final section, we take a broader perspective on superconductivity, stepping beyond the technical details to reflect on open problems that are currently attracting growing attentions. We also present two possible future directions, each linked to fundamental challenges in the physics of AMs and SC. While not exhaustive, these perspectives highlight the dynamic nature of the field and point toward areas where significant breakthroughs may soon emerge.

### A. Superconductivity in AM metals

The marriage between AFM and SC-exemplified by cuprates<sup>17</sup>, heavy fermions<sup>20</sup>, iron-based materials<sup>128–130</sup>, and more recently, infinite-layer nickelates<sup>131–133</sup>-stands as one of the most celebrated phenomena in physics. The emerging interplay between SC and AM metals may well enrich this family, offering a new arena where magnetism and SC are deeply intertwined<sup>92</sup>. As emphasized in the previous sections, the single-band Hamiltonian used to capture the spin-momentum locked FSs of AMs is only an approximation. A more realistic description must necessarily include the dual influence of strongly electron correlations from transition-metal cations and oriented ligands creating that create the anisotropic crystal field. When the ligand degree of freedom are integrated out, effective models emerge, in which the transition-metal ions residing at least two sublattices with anisotropic hoppings (see Eq.17). This multi-sublattice structure can be recognized as a defining feature of AMs. Indeed, recent theoretical works<sup>134–146</sup> have converged on the idea that incorporating such sublattice physics is important in understanding SC in AMs.

A striking demonstration of the influence of sublattice degree of freedom on the FFLO phases was provided by Sumita *et al.*<sup>142</sup>. To be specific, Sumita *et al.*<sup>142</sup> compared three different theoretical models in realizing FFLO states: a two-sublattice model with altermagnetic order (see Eq.19), a continuum model (see Eq.28), and a conventional square lattice model with spin-dependent hopping (see Eq.25a and Eq.25b). The key observation is that the latter two models, which do not account for the sublattice degree of freedom, consistently favor the LO states, whereas the first model prefers the FF states.

This suggests that the multi-sublattice nature plays a crucial role in enabling the emergence of AM-induced FF phase.

In 2023, Brekke *et al.*<sup>134</sup> proposed a two-dimensional minimal model to microscopically study the SC in AM. Unlike approaches that integrate out the ligand degree of freedom, this model explicitly incorporates them into the Hamiltonian. By analyzing the effective spin-spin exchange interactions mediated by ligands, the study reveals that the electron-magnon coupling can give rise to spin-polarized *p*-wave superconducting states. Moreover, the superconducting critical temperature can be substantially enhanced by tuning the chemical potential.

The combination of strongly electronic correlation and multi-orbital nature in AMs motivated Bose *et al.*<sup>136</sup> to investigate a multi-orbital *t* – *J* model, to be distinguished from the well studied single-band Hubbard and *t* – *J* model, which is believed to describe the interplay between AFM and SC in cuprates<sup>18</sup>. Using minimal *t* – *J* models on square-octagon lattices, the effect of doping and electron-electron interactions are investigated within the framework of mean-field theory. Bose *et al.*<sup>136</sup> uncovered a rich phase diagram comprising a variety of phases: metallic or insulating phases with strong AFM or AM order at half-filling, metallic phases with itinerant weak-coupling AM order or *d*-wave spin-density-wave states driven by quasi-one-dimensional van Hove singularities; and both *s*-wave and *d*-wave superconducting phases. Additionally, they identified regimes where AFM or AM order coexists with *d*-wave superconducting, giving rise to mixed singlet-triplet pairing. However, this coexistence appears unstable, tending toward phase separation into domains with Mott insulating order and domains with *d*-wave SC. In the presence of longer-range interactions, such phase separated states may organize into more structured pattern, such as stripes.

### B. Outlook: *p*-wave (unconventional) magnetism

While significant attention has been devoted to *d*-wave SML and AMs, their counterpart - *p*-wave SML and *p*-wave magnet - represent another important unconventional magnetism. Analogous to the *d*-wave SML, *p*-wave SML can either originate from PI in the spin channel<sup>12,36</sup> or be realized in certain AFMs<sup>147–158</sup>. Symmetry analysis on spin space groups elucidates that collinear magnets only support even-parity SML like *s*-wave in FMs, *d*-wave in AMs<sup>4</sup>. Consequently, the search for *p*-wave SML in magnetic materials must focus on non-collinear coplanar or noncoplanar systems.

In 2023, Hellenes *et al.*<sup>149</sup> revealed that  $[C_{2\perp}^{(s)}||\tau]$  in noncentrosymmetric non-collinear coplanar magnets can protect *p*-wave SML. It is important to note that in non-collinear coplanar magnets, the combination of  $C_{2\perp}^{(s)}$  and  $\tau$  gives  $\varepsilon(\mathbf{k}, \sigma_\perp, \sigma_\parallel) = \varepsilon(-\mathbf{k}, -\sigma_\perp, \sigma_\parallel)$ . Therefore, the effective  $\mathcal{P}$  present in collinear magnets is absent in non-collinear coplanar magnets. This breaking of  $\mathcal{P}$  im-

plies  $\varepsilon(\mathbf{k}, \sigma_\perp, \sigma_\parallel) \neq \varepsilon(-\mathbf{k}, \sigma_\perp, \sigma_\parallel)$ . Taken together, these symmetry considerations lead to *p*-wave SML, as illustrated in Fig.2(c). This insight has far-reaching implications, when SC is taken into account. The absence of  $\mathcal{P}$  naturally leads to non-centrosymmetric SC<sup>159</sup>, among which *p*-wave SC is especially sought after<sup>160–162</sup>. If such a symmetry condition are realized experimentally, they may offer a viable pathway to realizing topological SCs - highly desirable for their potential in fault-tolerant quantum computation. Therefore, exploring *p*-wave SML and *p*-wave magnets not only deepens our understanding of magnetism, but also paves the avenue toward technologically transformative superconducting phases.

### C. Outlook: multipole expansions of superconductivity

Beyond specific material realizations, there is significant potential to develop new conceptual frameworks. One particular promising direction involves extending the language of multipole expansions to superconductivity. As previously discussed, ELC phases can also describe Cooper pairs and since the language of ELC phases closely aligns with that of multipole expansions, it is naturally to consider applying the language of multipole expansions to Cooper pairs. In the context of multi-orbital SCs with SOC, this idea has already been explored by Nomoto *et al.*<sup>163</sup>, and the concept of multipole superconductivity was formally introduced by Sumita *et al.*<sup>164</sup>.

On a broader level, the multipole expansion framework provides a way to unify seemingly disparate superconducting orders under a single language, capturing not only conventional *s*-, *p*-, *d*-wave states but also more exotic pairing associated with higher-rang multipoles. Developing this framework further could therefore supply new guiding principles for identifying and classifying unconventional SCs, especially in AMs where orbital, spin, and lattice degree of freedom are intricately entangled. In this context, the multipole expansions of superconducting states by Kirikoshi *et al.*<sup>165</sup> represents not merely a mathematical reformulation but a conceptual leap that could reshape our understanding of paring in strongly correlated electron systems.

### DATA AVAILABILITY STATEMENT

The data is not available, because this is a review paper. The data cannot be made publicly available upon publication because they are owned by a third party and the terms of use prevent public distribution. The data that support the findings of this study are available upon reasonable request from the authors.

## ACKNOWLEDGMENTS

We thank H. Kusunose, H. Zhai and J. Wang for helpful discussions. This research was supported by the Australian Research Council's (ARC) Discovery Program, Grants Nos. DP240101590 (H.H.) and DP240100248 (X.-J.L.).

\* Corresponding author: zhaoliu@swin.edu.au

- <sup>1</sup> S. Hayami, Y. Yanagi, and H. Kusunose, Momentum-dependent spin splitting by collinear antiferromagnetic ordering. *J. Phys. Soc. Jpn.* **88**, 123702 (2019).
- <sup>2</sup> L.-D. Yuan, Z. Wang, J.-W. Luo, E. I. Rashba, and A. Zunger, Giant momentum-dependent spin splitting in centrosymmetric low-Z antiferromagnets. *Phys. Rev. B* **102**, 014422 (2020).
- <sup>3</sup> I. I. Mazin, K. Koepernik, M. D. Johannes, R. González-Hernández, and L. Šmejkal, Prediction of unconventional magnetism in doped FeSb<sub>2</sub>. *Proc. Natl. Acad. Sci. U.S.A.* **118**, e2108924118 (2021).
- <sup>4</sup> L. Šmejkal, J. Sinova, and T. Jungwirth, Beyond conventional ferromagnetism and antiferromagnetism: a phase with nonrelativistic spin and crystal rotation symmetry. *Phys. Rev. X* **12**, 031042 (2022).
- <sup>5</sup> L. Šmejkal, J. Sinova, and T. Jungwirth, Emerging Research Landscape of Altermagnetism. *Phys. Rev. X* **12**, 040501 (2022).
- <sup>6</sup> L. Bai, W. Feng, S. Liu, L. Šmejkal, Y. Mokrousov, and Y. Yao, Altermagnetism: exploring new frontiers in magnetism and spintronics. *Adv. Func. Mater.* **34**, 2409327 (2024).
- <sup>7</sup> C. Song, H. Bai, Z. Zhou, L. Han, H. Reichlova, J. H. Dil, J. Liu, X. Chen, and F. Han, Altermagnets as a new class of functional materials. *Nat. Rev. Mater.* **10**, 473-485 (2025).
- <sup>8</sup> Z. Guo, X. Wang, W. Wang, G. Zhang, X. Zhou, and Z. Cheng, Spin-polarized antiferromagnets for spintronics. *Adv. Mater.* **37**, 2505779 (2025).
- <sup>9</sup> T. Jungwirth, R. M. Fernandes, E. Fradkin, A. H. MacDonald, J. Sinova, and L. Šmejkal, Altermagnetism: an unconventional spin-ordered phase of matter. *Newton* **1**, 100162 (2025).
- <sup>10</sup> T. Jungwirth, J. Sinova, R. M. Fernandes, Q. Liu, H. Watanabe, S. Murakami, S. Nakatsui, and L. Šmejkal, Symmetry, microscopy and spectroscopy signatures of altermagnetism. arXiv:2506.22860.
- <sup>11</sup> T. Jungwirth, J. Sinova, P. Wadley, D. Kriegner, H. Reichlová, F. Krizek, H. Ohno, and L. Šmejkal, Altermagnetic spintronics. arXiv: 2508.09748.
- <sup>12</sup> C. Wu, S. Sun, E. Fradkin, and S.-C. Zhang, Fermi liquid instabilities in the spin channel. *Phys. Rev. B* **75**, 115103 (2007).
- <sup>13</sup> S. Hayami, M. Yatsushiro, Y. Yanagi, and H. Kusunose, Classification of atomic-scale multipoles under crystallographic point groups and application to linear response tensors. *Phys. Rev. B* **98**, 165110 (2018).
- <sup>14</sup> S. Hayami, Y. Yanagi, and H. Kusunose, Bottom-up design of spin-split and reshaped electronic band structures in antiferromagnets without spin-orbit coupling: procedure on the basis of augmented multipoles. *Phys. Rev. B* **102**, 144441 (2020).
- <sup>15</sup> P. Liu, J. Li, J. Han, X. Wan, and Q. Liu, Spin-group symmetry in magnetic materials with negligible spin-orbit coupling. *Phys. Rev. X* **12**, 021016 (2022).
- <sup>16</sup> S. A. Kivelson, E. Fradkin, and V. J. Emery, Electronic liquid-crystal phases of a doped Mott insulator. *Nature* **393**, 550-553 (1998).
- <sup>17</sup> J. G. Bednorz and K. A. Müller, Possible high T<sub>c</sub> superconductivity in the Ba-La-Cu-O system. *Z. Phys. B* **64**, 189-193 (1986).
- <sup>18</sup> P. A. Lee, N. Nagaosa and X.-G. Wen, Doping a Mott insulator: physics of high-temperature superconductivity. *Rev. Mod. Phys.* **78**, 17-85 (2006).
- <sup>19</sup> B. Keimer, S. A. Kivelson, M. R. Norman, S. Uchida and J. Zaanen, From quantum matter to high-temperature superconductivity in copper oxides. *Nature* **518**, 179-186 (2015).
- <sup>20</sup> F. Steglich, J. Aarts, C. D. Bredl, W. Lieke, D. Meschede, W. Franz, and H. Schäfer, Superconductivity in the presence of strong Pauli paramagnetism: CeCu<sub>2</sub>Si<sub>2</sub>. *Phys. Rev. Lett.* **43**, 1892 (1979).
- <sup>21</sup> G. R. Stewart, Heavy-fermion systems. *Rev. Mod. Phys.* **56**, 755 (1984).
- <sup>22</sup> P. Santini, S. Carretta, G. Amoretti, R. Caciuffo, N. Magnani, and G. H. Lander, Multipolar interactions in *f*-electron systems: the paradigm of actinide dioxides. *Rev. Mod. Phys.* **90**, 015005 (2009).
- <sup>23</sup> Y. Kuramoto, H. Kusunose, and A. Kiss, Multipole orders and fluctuations in strongly correlated electron systems. *J. Phys. Soc. Jpn.* **78**, 072001 (2009).
- <sup>24</sup> H. Kusunose and S. Hayami, Generalization of microscopic multipoles and cross-correlated phenomena by their ordering. *J. Phys.: Condens. Matter* **34**, 464002 (2022).
- <sup>25</sup> Unified description of electronic orderings and cross correlations by complete multipole representations. *J. Phys. Soc. Jpn.* **93**, 072001 (2024).
- <sup>26</sup> P. G. de Gennes and J. Prost, The physics of liquid crystals. *Oxford Science Publication/Clarendon Press Oxford*, UK (1993).
- <sup>27</sup> I. Ia. Pomeranchuk, On the stability of a Fermi liquid. *JETP* **8**, 361 (1958).
- <sup>28</sup> V. Oganesyan, S. A. Kivelson, and E. Fradkin, Quantum theory of a nematic Fermi fluid. *Phys. Rev. B* **64**, 195109 (2001).
- <sup>29</sup> H.-Y. Kee, E. H. Kim, and C.-H. Chung, Signatures of an electronic nematic phase at the isotropic-nematic phase transitions. *Phys. Rev. B* **68**, 245109 (2003).
- <sup>30</sup> I. Khavkine, C.-H. Chung, V. Oganesyan, and H.-Y. Kee, Formation of an electronic nematic phase in interacting fermion systems. *Phys. Rev. B* **70**, 155110 (2004).
- <sup>31</sup> H. Yamase, V. Oganesyan, and W. Metzner, Mean-field

- theory for symmetry-breaking Fermi surface deformations on a square lattice. *Phys. Rev. B* **70**, 155110 (2004).
- <sup>32</sup> C. A. Lamas, D. C. Cabra, and N. Grandi, Fermi liquid instabilities in two-dimensional lattice models. *Phys. Rev. B* **78**, 115104 (2008).
- <sup>33</sup> J. Quintanilla, M. Haque, and A. J. Schofield, Symmetry-breaking Fermi surface deformations from central interactions in two dimensions. *Phys. Rev. B* **78**, 035131 (2008).
- <sup>34</sup> E. C. Stoner, Collective electron ferromagnetism. *Proc. R. Soc. A* **165**, 372-414 (1938).
- <sup>35</sup> J. E. Hirsch, Spin-split states in metals. *Phys. Rev. B* **41**, 6820 (1990).
- <sup>36</sup> C. M. Varma and L. Zhu, Helicity order: hidden order parameter in URu<sub>2</sub>Si<sub>2</sub>. *Phys. Rev. Lett.* **96**, 036405 (2006).
- <sup>37</sup> T. T. M. Palstra, A. A. Menovsky, J. van den Berg, A. J. Dirkmaat, P. H. Kes, G. J. Nieuwenhuys, and J. A. Mydosh, Superconducting and magnetic transitions in the heavy-fermion system URu<sub>2</sub>Si<sub>2</sub>. *Phys. Rev. Lett.* **55**, 2727 (1985).
- <sup>38</sup> M. B. Maple, J. W. Chen, Y. Dalichaouch, T. Kohara, C. Rossel, M. S. Torikachvili, M. W. McElfresh, and J. D. Thompson, Helicity order: hidden order parameter in URu<sub>2</sub>Si<sub>2</sub>. *Phys. Rev. Lett.* **56**, 185 (1986).
- <sup>39</sup> C. Wu and S.-C. Zhang, Dynamic generation of spin-orbit coupling. *Phys. Rev. Lett.* **93**, 036403 (2004).
- <sup>40</sup> S. A. Kivelson, I. P. Bindloss, E. Fradkin, V. Oganesyan, J. M. Tranquada, A. Kapitulnik, and C. Howald, How to detect fluctuating stripes in the high-temperature superconductors. *Rev. Mod. Phys.* **75**, 1201 (2003).
- <sup>41</sup> C. Wu, Talk given by C. Wu at the Kavli Institute for Theoretical Physics on May 16, 2007. <https://online.kitp.ucsb.edu/online/colatoms07/wu1> (2007).
- <sup>42</sup> L. Fu, Parity-breaking phases of spin-orbit-coupled metals with gyroscopic, ferroelectric, and multipolar orders. *Phys. Rev. Lett.* **115**, 026401 (2015).
- <sup>43</sup> M. R. Norman, Dichroism as a probe for parity-breaking phases of spin-orbit coupled metals. *Phys. Rev. B* **92**, 075113 (2015).
- <sup>44</sup> J.-K. Yuan, Z. Pan, and C. Wu, Unconventional magnetism in spin-orbit coupled system. arXiv:2504.14577.
- <sup>45</sup> J. D. Jackson, Classical electrodynamics. *Wiley New York*, UK (1999).
- <sup>46</sup> V. M. Dubovik and A. A. Cheshkov, Multipole expansion in classical and quantum field theory and radiation. *Sov. J. Part. Nucl.* **5**, 318 (1975).
- <sup>47</sup> V. M. Dubovik and V. V. Tugushev, Toroidal moments in electronic dynamics and solid-state physics. *Phys. Rep.* **187**, 145-202 (1990).
- <sup>48</sup> N. A. Spaldin, M. Fiebig, and M. Mostovoy, The toroidal moment in condensed-matter physics and its relation to the magnetoelectric effect. *J. Phys.: Condens. Matter* **20**, 434203 (2008).
- <sup>49</sup> V. M. Dubovik, L. A. Tosunyan, and V. V. Tugushev, Axial toroidal moments in electrodynamics and solid-state physics. *Zh. Eksp. Teor. Fiz.* **90**, 590 (1986).
- <sup>50</sup> S. Nanz, Toroidal multipole moments in classical electrodynamics: an analysis of their emergence and physical significance. *Springer Berlin*, UK (2016).
- <sup>51</sup> S. Hayami and H. Kusunose, Microscopic description of electric and magnetic toroidal multipoles in hybrid orbitals. *J. Phys. Soc. Jpn.* **87**, 033709 (2018).
- <sup>52</sup> M.-T. Suzuki, T. Koretsune, M. Ochi, and R. Arita, Cluster multipole theory for anomalous Hall effect in antiferromagnets. *Phys. Rev. B* **96**, 094406 (2017).
- <sup>53</sup> M.-T. Suzuki, T. Nomoto, R. Arita, Y. Yanagi, S. Hayami, and H. Kusunose, Multipole expansion for magnetic structures: a generation scheme for a symmetry-adapted orthonormal basis set in the crystallographic point group. *Phys. Rev. B* **99**, 174407 (2019).
- <sup>54</sup> H. Watanabe and Y. Yanase, Group-theoretical classification of multipole order: emergent responses and candidate materials. *Phys. Rev. B* **98**, 245129 (2018).
- <sup>55</sup> T. Jungwirth, X. Marti, P. Wadley, and J. Wunderlich, Antiferromagnetic spintronics. *Nat. Nanotechnol.* **11**, 231-241 (2016).
- <sup>56</sup> V. Baltz, A. Manchon, M. Tsoi, T. Moriyama, T. Ono, and Y. Tserkovnyak, Antiferromagnetic spintronics. *Rev. Mod. Phys.* **90**, 015005 (2018).
- <sup>57</sup> S. Nakatsuji, N. Kiyohara, and T. Higo, Large anomalous Hall effect in a non-collinear antiferromagnet at room temperature. *Nature* **527**, 212-215 (2015).
- <sup>58</sup> H. Chen, P. Qin, H. Yan, Z. Feng, X. Zhou, X. Wang, Z. Meng, L. Liu, and Z. Liu, Noncollinear antiferromagnetic spintronics. *Materials Lab* **1**, 220032 (2022).
- <sup>59</sup> B. H. Rimmer, B. Pal, and S. S. P. Parkin Non-collinear antiferromagnetic spintronics. *Nat. Rev. Mater.* **10**, 109-127 (2025).
- <sup>60</sup> Y. Noda, K. Ohno, and S. Nakamura, Momentum-dependent band spin splitting in semiconducting MnO<sub>2</sub>: a density functional calculation. *Phys. Chem. Chem. Phys.* **18**, 13294-13303 (2016).
- <sup>61</sup> C. Franchini, R. Podlucky, J. Paier, M. Marsman, and G. Kresse, Ground-state properties of multivalent manganese oxides: density functional and hybrid density functional calculations. *Phys. Rev. B* **75**, 195128 (2007).
- <sup>62</sup> E. Cockayne and L. Li, First-principles DFT+U studies of the atomic, electronic, and magnetic structure of  $\alpha$ -MnO<sub>2</sub>. *Chem. Phys. Lett.* **544**, 53-58 (2012).
- <sup>63</sup> T. Okugawa, K. Ohno, Y. Noda, and S. Nakamura, Weakly spin-dependent band structures of antiferromagnetic perovskite LaMO<sub>3</sub> (M = Cr, Mn, Fe). *J. Phys.: Condens. Matter* **30**, 075502 (2018).
- <sup>64</sup> M. Naka, Y. Motome, and H. Seo, Altermagnetic perovskites. *npj Spintronics* **3**, 1 (2025).
- <sup>65</sup> M. Naka, S. Hayami, H. Kusunose, Y. Yanagi, Y. Motome, and H. Seo, Spin current generation in organic antiferromagnets. *Nat. Commun.* **10**, 4305 (2019).
- <sup>66</sup> K.-H. Ahn, A. Hariki, K.-W. Lee, and J. Kunes, Antiferromagnetism in RuO<sub>2</sub> as d-wave Pomeranchuk instability. *Phys. Rev. B* **99**, 184432 (2019).
- <sup>67</sup> L. Šmejkal, R. González-Hernández, T. Jungwirth, and J. Sinova, Crystal time-reversal symmetry breaking and spontaneous Hall effect in collinear antiferromagnets. *Sci. Adv.* **6**, eaaz8809 (2020).
- <sup>68</sup> S. A. Egorov, and R. A. Evarestov, Colossal spin splitting in the monolayer of the collinear antiferromagnet MnF<sub>2</sub>. *J. Phys. Chem. Lett.* **12**, 2363-2369 (2021).
- <sup>69</sup> H.-Y. Ma, M. Hu, N. Li, J. Liu, W. Yao, J.-F. Jia, and J. Liu, Multifunctional antiferromagnetic materials with giant piezomagnetism and noncollinear spin current. *Nat. Commun.* **12**, 2846 (2021).
- <sup>70</sup> D.-F. Shao, S.-H. Zhang, M. Li, C.-B. Eom, and E. Y. Tsymbal, Spin-neutral currents for spintronics. *Nat. Commun.* **12**, 7061 (2021).
- <sup>71</sup> R. González-Hernández, L. Šmejkal, K. Výborný, Y. Yahagi, J. Sinova, T. Jungwirth, and J. Železný, Efficient electrical spin splitter based on nonrelativistic collinear

- antiferromagnetism. *Phys. Rev. Lett.* **126**, 127701 (2021).
- <sup>72</sup> L. Šmejkal, A. B. Hellenes, R. González-Hernández, J. Sinova, and T. Jungwirth, Giant and tunneling magnetoresistance in unconventional collinear antiferromagnets with nonrelativistic spin-momentum locking. *Phys. Rev. X* **12**, 011028 (2022).
- <sup>73</sup> I. Mazin, Editorial: altermagnetism-a new punch line of fundamental magnetism. *Phys. Rev. X* **12**, 040002 (2022).
- <sup>74</sup> Q. Liu, X. Dai, and S. Blügel, Different facets of unconventional magnetism. *Nat. Phys.* **21**, 329-331 (2025).
- <sup>75</sup> S.-W. Cheong and F.-T. Huang, Altermagnetism with non-collinear spins. *npj Quantum Mater.* **9**, 13 (2024).
- <sup>76</sup> S.-W. Cheong and F.-T. Huang, Altermagnetism classification. *npj Quantum Mater.* **10**, 38 (2025).
- <sup>77</sup> P. Das, V. Leeb, J. Knolle, and M. Knap, Realizing altermagnetism in Fermi-Hubbard models with ultracold atoms. *Phys. Rev. Lett.* **132**, 263402 (2024).
- <sup>78</sup> P. A. McClarty and J. G. Rau, Landau theory of altermagnetism. *Phys. Rev. Lett.* **132**, 176702 (2024).
- <sup>79</sup> M. Roig, A. Kreisel, Y. Yu, B. M. Andersen, and D. F. Agterberg, Minimal models for altermagnetism. *Phys. Rev. B* **110**, 144412 (2024).
- <sup>80</sup> V. E. Naish, On magnetic symmetry of crystals. *Proc. USSR Acad. Sci.* **27**, 1496 (1963).
- <sup>81</sup> A. Kitz, Über die symmetriegruppen von spinverteilungen von. *Phys. Status Solidi (b)* **10**, 455 (1965).
- <sup>82</sup> W. F. Brinkman and R. J. Elliott, Theory of spin-space groups. *Proc. R. Soc. A* **294**, 343 (1966).
- <sup>83</sup> W. F. Brinkman and R. J. Elliott, Space grou theory for spin waves. *J. Appl. Phys.* **37**, 1457 (1966).
- <sup>84</sup> D. B. Litvin, Spin translation groups and neutron diffraction analysis. *Acta Crystallogr. Sect. A* **29**, 651 (1973).
- <sup>85</sup> D. B. Litvin and W. Opechowski, Spin groups. *Physica* **76**, 538 (1974).
- <sup>86</sup> D. B. Litvin, Spin point groups. *Acta Crystallogr. Sect. A* **33**, 279 (1977).
- <sup>87</sup> Z. Xiao, J. Zhao, Y. Li, R. Shindou, and Z.-D. Song, Spin space groups: full classification and applications. *Phys. Rev. X* **14**, 031037 (2024).
- <sup>88</sup> X. Chen, J. Ren, Y. Zhu, Y. Yu, A. Zhang, P. Liu, J. Li, Y. Liu, C. Li, and Q. Liu, Enumeration and representation theory of spin space groups. *Phys. Rev. X* **14**, 031038 (2024).
- <sup>89</sup> Y. Jiang, Z. Song, T. Zhu, Z. Fang, H. Weng, Z.-X. Liu, J. Yang, and C. Fang, Enumeration of spin-space groups: towards a complete description of symmetries of magnetic orders. *Phys. Rev. X* **14**, 031039 (2024).
- <sup>90</sup> P. Fulde and R. A. Ferrell, Superconductivity in a Strong Spin-Exchange Field. *Phys. Rev.* **135**, A550 (1964).
- <sup>91</sup> A. I. Larkin and Yu. N. Ovchinnikov, Nonuniform state of superconductors. *Zh. Eksp. Teor. Fiz.* **47**, 1136 (1964) [*Sov. Phys. JETP* **20**, 762 (1965)].
- <sup>92</sup> I. I. Mazin, Notes on altermagnetism and superconductivity. *AAPPS Bulletin* **35**, 8 (2025).
- <sup>93</sup> S. Banerjee and M. S. Scheurer, Altermagnetic superconducting diode effect. *Phys. Rev. B* **110**, 024503 (2024).
- <sup>94</sup> Q. Cheng, Y. Mao, and Q.-F. Sun, Field-free Josephson diode effect in altermagnet/normal metal/altermagnet junctions. *Phys. Rev. B* **110**, 014518 (2024).
- <sup>95</sup> G. Sim and J. Knolle, Pair density wave and supercurrent diode effect in altermagnets. *Phys. Rev. B* **112**, L020502 (2025).
- <sup>96</sup> D. Chakraborty and A. M. Black-Schaffer, Perfect superconducting diode effect in altermagnets. *Phys. Rev. Lett.* **135**, 026001 (2025).
- <sup>97</sup> F. Yang and L. Q. Chen, Altermagnetism-induced non-collinear superconducting diode effect and unidirectional superconducting transport. arXiv: 2507.05543.
- <sup>98</sup> J. A. Ouassou, A. Brataas, and J. Linder, dc Josephson effect in altermagnets. *Phys. Rev. Lett.* **131**, 076003 (2023).
- <sup>99</sup> B. Lu, K. Maeda, H. Ito, K. Yada, and Y. Tanaka,  $\varphi$  Josephson junction induced by altermagnetism. *Phys. Rev. Lett.* **133**, 226002 (2024).
- <sup>100</sup> Q. Cheng and Q.-F. Sun, Orientation-dependent Josephson effect in spin-singlet superconductor/altermagnet/spin-singlet superconductor junctions. *Phys. Rev. B* **109**, 024517 (2024).
- <sup>101</sup> Y. Fukaya, K. Maeda, K. Yada, J. Cayao, Y. Tanaka, and B. Lu, Josephson effect and odd-frequency pairing in superconducting junctions with unconventional magnets. *Phys. Rev. B* **111**, 064502 (2025).
- <sup>102</sup> W. Zhao, Y. Fukaya, P. Burset, J. Cayao, Y. Tanaka, and B. Lu, Orientation-dependent transport in junctions formed by  $d$ -wave altermagnets and  $d$ -wave superconductors. *Phys. Rev. B* **111**, 184515 (2025).
- <sup>103</sup> A. Boruah, S. Acharjee, and P. K. Saikia, Field-free Josephson diode effect in an Ising-superconductor/altermagnet/Ising-superconductor Josephson junction. *Phys. Rev. B* **112**, 045505 (2025).
- <sup>104</sup> M. Papaj, Andreev reflection at the altermagnet-superconductor interface. *Phys. Rev. B* **108**, L060508 (2023).
- <sup>105</sup> C. Sun, A. Brataas, and J. Linder, Andreev reflection in altermagnets. *Phys. Rev. B* **108**, 054511 (2023).
- <sup>106</sup> S. Das and A. Soori, Crossed Andreev reflection in altermagnets. *Phys. Rev. B* **109**, 245424 (2024).
- <sup>107</sup> D. Yu Kazmin, V. D. Esin, Yu. S. Barash, A. V. Timonina, N. N. Kolesnikov, and E. V. Deviatov, Andreev reflection for MnTe altermagnet candidate. *Phys. B: Condens. Matter* **696**, 416602 (2025).
- <sup>108</sup> Y.-X. Li and C.-C. Liu, Majorana corner modes and tunable patterns in an altermagnet heterostructure. *Phys. Rev. B* **108**, 205410 (2023).
- <sup>109</sup> Y.-X. Li, Realizing tunable higher-order topological superconductors with altermagnets. *Phys. Rev. B* **109**, 224502 (2024).
- <sup>110</sup> S. A. A. Ghorashi, T. L. Hughes, and J. Cano, Altermagnetic routes to Majorana modes in zero net magnetization. *Phys. Rev. Lett.* **133**, 106601 (2024).
- <sup>111</sup> D. Mondal, A. Pal, A. Saha, and T. Nag, Distinguish between topological Majorana and trivial zero modes via transport and shot noise study in an altermagnet heterostructure. *Phys. Rev. B* **111**, L121401 (2025).
- <sup>112</sup> T. Hodge, E. Mascot, and S. Rachel, Altermagnet-superconductor heterostructure: a scalable platform for braiding of Majorana modes. arXiv: 2506.08095.
- <sup>113</sup> A. Pal, D. Mondal, T. Nag, and A. Saha, Josephson current signature of Floquet Majorana and topological accidental zero modes in altermagnet heterostructure. arXiv: 2505.05302.
- <sup>114</sup> P.-H. Fu, S. Mondal, J.-F. Liu, Y. Tanaka, and J. Cayao, Floquet engineering spin triplet states in unconventional magnets. arXiv: 2505.20205.
- <sup>115</sup> P.-H. Fu, S. Mondal, J.-F. Liu, and J. Cayao, Light-induced Floquet spin-triplet Cooper pairs in unconventional magnets. arXiv: 2506.10590.
- <sup>116</sup> Y. Fukaya, B. Lu, K. Yada, Y. Tanaka, and J. Cayao

- Superconducting phenomena in systems with unconventional magnets. *J. Phys.: Condens. Matter* **37**, 313003 (2025).
- <sup>117</sup> A. E. Feiguin and M. P. A. Fisher, Exotic paired states with anisotropic spin-dependent Fermi surfaces. *Phys. Rev. Lett.* **103**, 025303 (2009).
- <sup>118</sup> G. E. Volovik, Superconductivity with lines of gap nodes: density of states in the vortex. *Zh. Eksp. Teor. Fiz.* **58**, 457 (1993) [*JETP Lett.* **58**, 469 (1993)].
- <sup>119</sup> R. Soto-Garrido and E. Fradkin, Pair-density-wave superconducting states and electronic liquid-crystal phases. *Phys. Rev. B* **89**, 165126 (2014).
- <sup>120</sup> D. Chakraborty and A. M. Black-Schaffer, Zero-field finite-momentum and field-induced superconductivity in altermagnets. *Phys. Rev. B* **110**, L060508 (2024).
- <sup>121</sup> S.-B. Zhang, L.-H. Hu, and T. Neupert, Finite-momentum Cooper pairing in proximitized altermagnets. *Nat. Commun.* **15**, 1801 (2024).
- <sup>122</sup> Z. Liu, H. Hu, and X.-J. Liu, Fulde-Ferrell-Larkin-Ovchinnikov states and topological Bogoliubov Fermi surfaces in altermagnets: an analytical study. arXiv:2508.07813.
- <sup>123</sup> S. Hong, M. J. Park, and K.-M. Kim, Unconventional *p*-wave and finite-momentum superconductivity induced by altermagnetism through the formation of Bogoliubov Fermi surface. *Phys. Rev. B* **111**, 054501 (2025).
- <sup>124</sup> H. Hu, Z. Liu, and X.-J. Liu, Unconventional superconductivity of an altermagnetic metal: polarized BCS and inhomogeneous Fulde-Ferrell-Larkin-Ovchinnikov states. arXiv:2505.10196.
- <sup>125</sup> M. Sigrist and K. Ueda, Phenomenological theory of unconventional superconductivity. *Rev. Mod. Phys.* **63**, 239 (1991).
- <sup>126</sup> J. Gukelberger, E. Kozik, L. Pollet, N. Prokif'ev, M. Sigrist, B. Svistunov, and M. Troyer, *p*-wave superfluidity by spin-nematic Fermi surface deformation. *Phys. Rev. Lett.* **113**, 195301 (2014).
- <sup>127</sup> D. Zhu, Z.-Y. Zhuang, Z. Wu, and Z. Yan, Topological superconductivity in two-dimensional altermagnetic metals. *Phys. Rev. B* **108**, 184505 (2023).
- <sup>128</sup> Y. Kamihara, T. Watanabe, M. Hitano, and H. Hosono, Iron-based layered superconductor La(O<sub>1-x</sub>F<sub>x</sub>)FeAs (x=0.05-0.12) with *T<sub>c</sub>* = 26 K. *J. Am. Chem. Soc.* **130**, 3296-3297 (2008).
- <sup>129</sup> Q.-Y. Wang, Z. Li, W.-H. Zhang, Z.-C. Zhang, J.-S. Zhang, W. Li, H. Ding, Y.-B. Ou, P. Deng, K. Chang, J. Wen, C.-L. Song, K. He, J.-F. Jia, S.-H. Ji, Y.-Y. Wang, L.-L. Wang, X. Chen, X.-C. Ma, and Q.-K. Xue, Interfacial-induced high-temperature superconductivity in single unit-cell FeSe films on SrTiO<sub>3</sub>. *Chin. Phys. Lett.* **29**, 037402 (2012).
- <sup>130</sup> P. Dai, Antiferromagnetic order and spin dynamics in iron-based superconductors. *Rev. Mod. Phys.* **87**, 855 (2015).
- <sup>131</sup> D. Li, J. Lee, B. Y. Wang, M. Osada, S. Crossley, H. R. Lee, Y. Cui, Y. Hikita, and H. Y. Hwang, Superconductivity in an infinite-layer nickelate. *Nature* **572**, 624-627 (2019).
- <sup>132</sup> Z. Liu, Z. Ren, W. Zhu, Z. Wang, and J. Yang, Electronic and magnetic structure of infinite-layer NdNiO<sub>2</sub>: trace of antiferromagnetic metal. *npj Quantum Mater.* **5**, 31 (2020).
- <sup>133</sup> H. Lu, M. Rossi, A. Nag, M. Osada, D. F. Li, K. Lee, B. Y. Wang, M. Garcia-Fernandez, S. Agrestini, Z. X. Shen, E. M. Been, B. Moritz, T. P. Devereaux, J. Zaanen, H. Y. Hwang, K.-J. Zhou, and W. S. Lee, Magnetic excitations in infinite-layer nickelates. *Science* **373**, 213-216 (2021).
- <sup>134</sup> B. Brekke, A. Brataas, and A. Sudbø, Two-dimensional altermagnets: superconductivity in a minimal microscopic model. *Phys. Rev. B* **108**, 224421 (2023).
- <sup>135</sup> S. Sumita, M. Naka, and H. Seo, Fulde-Ferrell-Larkin-Ovchinnikov state induced by antiferromagnetic order in  $\kappa$ -type organic conductors. *Phys. Rev. Res.* **5**, 043171 (2023).
- <sup>136</sup> A. Bose, S. Vadnais, and A. Paramekanti, Altermagnetism and superconductivity in a multiorbital t-J model. *Phys. Rev. B* **110**, 205120 (2024).
- <sup>137</sup> A. Mæland, B. Brekke, and A. Sudbø, Many-body effects on superconductivity mediated by double-magnon processes in altermagnets. *Phys. Rev. B* **109**, 134515 (2024).
- <sup>138</sup> K. Leraand, A. Mæland, and A. Sudbø, Phonon-mediated spin-polarized superconductivity in altermagnets. arXiv: 2502.08704.
- <sup>139</sup> D. Chakraborty and A. M. Black-Schaffer, Constraints on superconducting pairing in altermagnets. *Phys. Rev. B* **112**, 014516 (2025).
- <sup>140</sup> N. Parthenios, P. M. Bonetti, R. González-Hernández, W. H. Campos, L. Šmejkal, and L. Classen, Spin and pair density waves in 2D altermagnetic metals. arXiv:2502.19270.
- <sup>141</sup> Y.-M. Wu, Y. Wang, and R. M. Fernandes, Intra-unit-cell singlet pairing mediated by altermagnetic fluctuations. arXiv: 2506.04356.
- <sup>142</sup> S. Sumita, M. Naka, and H. Seo, Phase-modulated superconductivity via altermagnetism. arXiv:2506.22297.
- <sup>143</sup> X. Feng and Z. Zhang, Superconducting order parameters in spin space groups: methodology and application. arXiv:2407.20504.
- <sup>144</sup> K. Maeda, Y. Fukaya, K. Yada, B. Lu, Y. Tanaka, and J. Cayao, Classification of pair symmetries in superconductors with unconventional magnetism. *Phys. Rev. B* **111**, 144508 (2025).
- <sup>145</sup> K. Parshukov and A. P. Schnyder, Exotic superconducting states in altermagnets. arXiv:2507.10700.
- <sup>146</sup> C. L. H. Rasmussen, J. Gondolf, M. Barkman, M. Roig, D. F. Agterberg, A. Kreisel, and B. M. Andersen, Inherent momentum-dependent gap structure of altermagnetic superconductors. arXiv:2509.03247.
- <sup>147</sup> S. Hayami, Y. Yanagi, and H. Kusunose, Spontaneous antisymmetric spin splitting in noncollinear antiferromagnets without spin-orbit coupling. *Phys. Rev. B* **101**, 220403(R) (2020).
- <sup>148</sup> S. Hayami, Mechanism of antisymmetric spin polarization in centrosymmetric multipole-*Q* magnets based on effective chiral bilinear and biquadratic spin cross products. *Phys. Rev. B* **105**, 024413 (2022).
- <sup>149</sup> A. B. Hellénnes, T. Jungwirth, R. Jaeschke-Ubiergo, A. Chakraborty, and L. Šmejkal, *P*-wave magnets. arXiv:2309.01607.
- <sup>150</sup> Q. Song, S. Stavrić, P. Barone, A. Droghetti, D. S. Antonenko, J. W. F. Venderbos, C. A. Occhialini, B. Ilyas, E. Ergençen, N. Gedik, S.-W. Cheong, R. M. Fernandes, S. Picozzi, and R. Comin, Electrical switching of a *p*-wave magnet. *Nature* **642**, 64-70 (2025).
- <sup>151</sup> A. Chakraborty, A. B. Hellénnes, R. Jaeschke-Ubiergo, T. Jungwirth, L. Šmejkal, and J. Sinova, Highly efficient non-relativistic Edelstein effect in nodal *p*-wave magnets. *Nat. Commun.* **16**, 7270 (2025).

- <sup>152</sup> Y. Yu, M. B. Lyngby, T. Shishidou, M. Roig, A. Kreisel, M. Weinert, B. M. Andersen, and D. F. Agterberg, Odd-parity magnetism derived by antiferromagnetic exchange. *Phys. Rev. Lett.* **135**, 046701 (2025).
- <sup>153</sup> B. Brekke, P. Sukhachov, H. G. Giil, A. Brataas, and J. Linder, Minimal models and transport properties of unconventional *p*-wave magnets. *Phys. Rev. Lett.* **133**, 236703 (2024).
- <sup>154</sup> M. Ezawa, Topological insulators and superconductors based on *p*-wave magnets: electrical control and detection of a domain wall. *Phys. Rev. B* **110**, 165429 (2024).
- <sup>155</sup> Z.-Y. Zhuang, D. Zhu, D. Liu, Z. Wu, and Z. Yan, Odd-parity altermagnetism originated from orbital orders. arXiv:2508.18361.
- <sup>156</sup> S. Huang, Z. Qin, F. Zhan, D.-H. Xu, D.-S. Ma, and R. Wang, Light-induced odd-parity magnetism in conventional collinear antiferromagnets. arXiv:2507.20705.
- <sup>157</sup> T. Zhu, D. Zhou, H. Wang, and J. Ruan, Floquet odd-parity collinear magnets. arXiv:2508.02542.
- <sup>158</sup> D. Liu, Z.-Y. Zhuang, D. Zhu, Z. Wu, and Z. Yan, Light-induced odd-parity altermagnets on dimerized lattices. arXiv:2508.18360.
- <sup>159</sup> E. Baur, M. Sigrist eds., Non-centrosymmetric superconductors: introduction and overview. *Springer Science & Business Media Berlin/Heidelberg*, (2012).
- <sup>160</sup> Y. Nagae, L. Katayama, and S. Ikegaya, Flat-band zero-energy states and anomalous proximity effects in *p*-wave magnet-superconductor hybrid systems. *Phys. Rev. B* **111**, 174519 (2025).
- <sup>161</sup> P. Sukhachov, H. G. Giil, B. Brekke, and J. Linder, Coexistence of *p*-wave magnetism and superconductivity. *Phys. Rev. B* **111**, L220403 (2025).
- <sup>162</sup> Z.-T. Sun, X. Feng, Y.-M. Xie, B. T. Zhou, J.-X. Hu, and K. T. Law, Pseudo-Ising superconductivity induced by *p*-wave magnetism. arXiv:2501.10960.
- <sup>163</sup> T. Nomoto, K. Hattori, and H. Ikeda, Classification of "multipole" superconductivity in multiorbital systems and its implications. *Phys. Rev. B* **94**, 174513 (2016).
- <sup>164</sup> S. Sumita, T. Nomoto, and Y. Yanase, Multipole superconductivity in nonsymmorphic Sr<sub>2</sub>IrO<sub>4</sub>. *Phys. Rev. Lett.* **119**, 027001 (2017).
- <sup>165</sup> A. Kirikoshi and S. Hayami, Classification of multiorbital superconducting state based on augmented multipoles. *Phys. Rev. B* **109**, 174510 (2024).